Solvent-Mediated Charge Transfer Dynamics of a Model Brown Carbon Aerosol Chromophore: Photophysics of 1-Phenylpyrrole Induced by Water Solvation

Brianna N. Peterson,[1] Megan E. Alfieri,[1] David J. Hood,[1] Christian D. Hettwer,[1] Daniel V. Costantino,[1] Daniel P. Tabor,[2,a] Nathanael M. Kidwell[1,a]

[1] *Department of Chemistry, The College of William and Mary, Williamsburg, VA 23187-8795, USA*

[2] *Department of Chemistry, Texas A&M University, College Station, TX 77843, USA*

Abstract

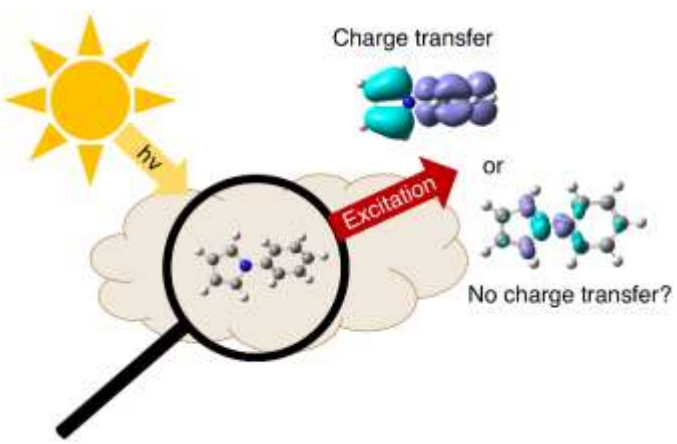

Nitrogen heterocycles are known to be important light-absorbing chromophores in a relatively new class of aerosols, commonly referred to as 'brown carbon' (BrC) aerosols. Due to their significant absorption and spectral overlap with the solar actinic flux, these BrC chromophores steer the physical and optical properties of aerosols. To model the local aqueous solvation environment surrounding BrC chromophores, we generated cold molecular complexes with water and a prototypical BrC chromophore, 1-phenylpyrrole (1PhPy), using supersonic jet-cooling and explored their intermolecular interactions using single-conformation spectroscopy. Herein, we utilized resonant two-photon ionization (R2PI) and UV holeburning (UV HB) double-resonance spectroscopies to obtain a molecular-level understanding of water microsolvation's role in charge transfer upon photoexcitation of 1PhPy. Quantum chemical calculations and one-dimensional discrete variable representation simulations revealed insights into the charge transfer efficacy of 1PhPy with and without single water molecule addition. Taken together, our results indicate that the intermolecular interactions with water guide the geometry of 1PhPy to adopt a more twisted intramolecular charge transfer (TICT) configuration, thus facilitating charge transfer from the pyrrole donor to the phenyl ring acceptor. Fluorescence measurements with increasing H_2O %volume corroborated our gas-phase studies by indicating that a polar water solvation environment stabilizes the TICT configuration of 1PhPy in the excited electronic state, from which emission is observed at lower energy compared to the locally-excited configuration.

* Correspondence email: nmkidwell@wm.edu; daniel_tabor@tamu.edu

Introduction

Water-mediated interactions determine the structural, dynamical, and optical properties of aqueous solutions and interfaces,[1,2] which play a key role in biological folding,[3–5] photosynthetic energy conversion,[6–8] and aerosol solar absorption.[9–11] Considering the ubiquity of water-mediated interactions in numerous environments, there remain longstanding questions regarding how solvation shapes the photophysics of the solute partner. Thus, a fundamental description of the intermolecular interactions between the chromophore solute and H_2O solvent is still far from complete. The spatial configurations of solute-$(H_2O)_n$ molecular complexes offer exquisite insights not only into the nature of hydrogen bonding forces that influence their stability, but they also serve as essential tools for understanding and modeling condensed phase environments. In this view, molecular complexes act as a bridge between the gas and condensed phases.[12,13] The configurations of complexes provide a molecular-level understanding of solvation surrounding chromophore solutes in water networks that mimic air-liquid interfaces, leading to insights on their physical properties. Hydrogen-bonded molecular complexes occupy an interesting size regime large enough to exhibit significant complexity, but small enough that their potential energy surfaces can still be explored in some detail by experimental methods and modern theoretical methods. Indeed, aerosol solar absorption is steered by the photophysics and photochemistry of light-absorbing chromophores embedded within the aqueous environment of aerosols.

Aerosols are suspensions of fine liquid or solid particles in the atmosphere that impact public health, climate, and energy balance.[14] Carbonaceous aerosols are divided into distinct classifications depending on whether they are light absorbing (black and brown carbon) or light scattering (organic carbon).[15,16] Black carbon (BC) aerosol absorption does not vary with wavelength, whereas the absorption propensity of brown carbon (BrC) aerosols is highly

dependent on wavelength with a smooth absorption increase from the visible to ultraviolet range.[17] BrC aerosols enhance light absorption and water evaporation that are key events to understanding the intricate relationships between clouds, aerosols, and global climate. The effects of clouds and aerosols are presently a major source of uncertainty in global climate and global atmospheric chemistry models.[18,19] In fact, it has been estimated[20] that BrC aerosols are responsible for up to 24% of radiative forcing that was previously thought to be from BC aerosols. Nitrogen heterocycles (*N*-heterocycles) have recently been identified as key light-absorbing chromophores in BrC aerosols.[21] Due to their significant absorption strengths and overlap with the solar flux, *N*-heterocycles shape the optical properties of BrC aerosols and global climate, even in low concentrations.

Pyrrole and pyrrole derivatives fulfill many of the common structural motifs identified as BrC chromophores.[21] There is also supporting evidence that intramolecular charge transfer (ICT) complexes may contribute to BrC aerosols due to their large transition dipole moment resulting in increased molar absorptivity.[22] 1-Phenylpyrrole (1PhPy) shown in Figure 1 is a model BrC chromophore and a plausible ICT molecule. Upon excitation of 1PhPy, electron charge transfer is initiated from the pyrrole π orbital donor to the phenyl ring π^* orbital acceptor. However, large amplitude motion along the CN-CC torsional coordinate (highlighted in Figure 1) affects the degree to which charge transfer occurs. Electron donor/acceptor molecules can emit fluorescence from two relaxed singlet excited states (dual fluorescence). Upon photoexcitation, a locally-excited state (LE) is formed, from which an ICT state with a larger dipole moment is generated. Dual fluorescence from electronic excitation of 1PhPy has been observed in nonpolar and polar solvents.[23,24] The two fluorescence bands have been attributed to radiative emission from an LE state configuration obtained at various dihedral angles, whereas a perpendicular (CN-CC dihedral

= 90°) geometry, often referred to as a twisted intramolecular charge transfer (TICT) configuration, is responsible for the red-shifted emission band. Polar solvents such as water may therefore stabilize the TICT geometry and the charge distribution following photoexcitation. In a two-fold rotation scheme, CN-CC dihedral angles = 0° or ±90° are regarded as having planar or perpendicular geometries, respectively, with barriers for torsional interconversion, ΔE_0 and ΔE_{90}.

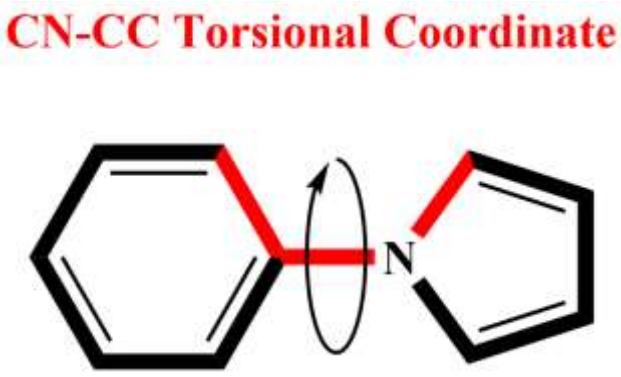

Figure 1: The structure of 1PhPy with the dihedral angle of interest highlighted.

Previous works have characterized the extent to which 1PhPy undergoes isomerization in the excited state from the LE geometry to the TICT structure. Okuyama et al.[25] recorded the ground and excited state vibronic spectra of the bare 1PhPy chromophore under jet-cooled conditions and fit the data with a Franck-Condon simulation analysis to determine torsional potential energy surfaces. Since the simulations yielded ΔE_{90} that was larger than ΔE_0 in the excited state, the authors concluded that 1PhPy does not adopt a perpendicular TICT geometry. Thomas et al. obtained the rotationally-resolved spectrum of isolated 1PhPy in a molecular beam under an applied electric field, and complemented experiments with calculations at the M05-2X/6-31G level of theory.[26] Their study found that the permanent electric dipole moment in the more planar ^1L_b excited state is reversed from the ground state, with the $\Delta\mu \sim 2.5$ Debye resulting from ~0.15 e^- charge transfer from the pyrrole to the phenyl ring upon excitation. Carrying out theoretical

calculations at the CASSCF/CASPT2 level of theory, Proppe and co-workers[27] determined that when 1PhPy is placed in acetonitrile solvent, ΔE_{90} is reduced, thus preferring a TICT geometry from which emission occurs at approximately 3.72 eV. In a follow up study,[28] Manz utilized non-equilibrium molecular dynamics simulations to study the dynamics of 1PhPy in acetonitrile solvent, and concluded that the TICT isomerization occurred on a 5-10 ps timescale, with rapid acetonitrile solvent reorganization on the order of 100 fs. More recently, the absorption and fluorescence of 1PhPy in the gas phase and in acetonitrile was carried out by Aguilar et al at the CASPT2//CASSCF level, where they identified a stabilized TICT conformation in acetonitrile with a very flat free energy surface.[29] Furthermore, Schweke et al[30] generated 1PhPy + acetonitrile complexes in an argon matrix and determined that 1PhPy behaved with TICT character as a complex.

The focus of this article is to determine the structural details of the charge transfer mechanism of 1PhPy in the absence and presence of water as a polar solvent to mimic the aqueous environment of BrC aerosols. Using mass-resolved spectroscopy and double-resonance methods in tandem with theoretical calculations, the intermolecular interactions of 1PhPy with water were investigated. Our goal is to reveal water's role in shaping the charge transfer mechanism induced from electronic excitation of 1PhPy and whether a TICT spatial configuration is preferred in the hydrogen bond network with water. Therefore, we aim to investigate these fundamental processes from the bottom-up to further understand the solar absorption outcomes of BrC chromophores and to model the local solvation environment surrounding BrC chromophores found in aerosols. Interpretation of the experimental spectra is aided by modeling the spectra from the energies and torsional wavefunctions calculated via discrete variable representation (DVR) calculations on the torsional potential energy surface. The DVR family of methods is useful for calculating the

energies of arbitrary low-dimensional potentials, as the methods can be numerically converged by reducing the grid spacing. Fluorescence emission measurements recorded with increasing H_2O %volume report on the intramolecular charge transfer dynamics of 1PhPy in the condensed phase, translating more directly to the solar absorption outcomes of BrC aerosols.

Experimental Methods

1-Phenylpyrrole (1PhPy) was purchased from Sigma-Aldrich (99%) and used without further purification. All experiments were carried out in a custom-built chamber described previously.[31] 1PhPy was placed into a stainless-steel reservoir behind a 500 µm pulse valve nozzle (Series 9 General Valve) operating at 10 Hz and heated to 40 °C to obtain sufficient vapor pressure. The entire gas manifold is comprised of two independent gas channels, wherein a single gas line containing helium (He; ~2-3 bar backing pressure) is split into a pure He gas channel to entrain the 1PhPy sample and another channel containing a reservoir with water to seed into the gas expansion. The two channels re-converge prior to the 1PhPy sample container. Water complexes with 1PhPy were selectively generated by opening a gas shutoff valve to the water gas channel, and the gas flow was fine-tuned with a needle valve to optimize experimental conditions. Using a mass flow meter (Teledyne Hastings), the 1PhPy sample gas flow, water gas flow, and total gas flow were monitored to determine molecular number densities (~0.05 % water). The gas mixture with or without water present was pulsed into a high-vacuum time-of-flight mass spectrometer, creating a molecular beam and adiabatically cooling 1PhPy or 1PhPy + nH_2O complexes to their respective zero-point vibrational levels by supersonic jet expansion. A skimmer (2mm; Beam Dynamics) was placed at a distance of 30 mm from the pulse nozzle to select the molecules or complexes with the lowest internal energy prior to laser interrogation.

In the collision-free region of the expansion downstream, the skimmed molecular beam is probed with resonant two-photon ionization (R2PI) spectroscopy to obtain vibrationally-resolved excitation spectra out of the ground-state zero-point level with mass selectivity. Tunable ultraviolet (UV) light was generated by frequency-doubling the output of a Nd:YAG pumped dye laser (Radiant Dyes NarrowScan) with an Inrad Autotracker III equipped with a BBO crystal. The excited state spectra were obtained by UV exciting 1PhPy or 1PhPy + $1H_2O$ to vibronic levels with the probe laser (10 Hz), from which the excited state population was ionized using the same UV light source. The mass ion signal was gated and monitored as a function of the probe UV wavelength to generate the R2PI spectrum.

The R2PI spectrum is frequently the sum of contributions arising from multiple conformational isomers or fragments from photoionization of molecular complexes, which can be deconvoluted using ultraviolet holeburning (UV HB) double-resonance spectroscopy. Here, a holeburn laser (5 Hz) is spatially overlapped with the probe laser from the R2PI method and precedes the probe laser by 50 ns. The holeburn laser was fixed on and partially saturated specific vibronic features in the R2PI spectra due to a conformational or complex isomer, thus removing a sizeable fraction of the ground state population. As the probe laser is scanned and becomes resonant with a shared ground state transition as the holeburn laser, the isomer ground state population is depleted. A difference spectrum is obtained by monitoring the gated mass ion probe signal using active baseline subtraction and averaging the signal depletion with the probe wavelength.

Next, condensed-phase fluorescence emission and excitation measurements of 1PhPy in varying solvent concentrations were obtained. Standard solutions of varying polarity were prepared using tetrahydrofuran (Fisher-Scientific, 100%) and ultra-pure water. Solutions were

made in the %volume ratios of THF:H_2O of 100:0, 80:20, 60:40, 40:60 and 20:80. Approximately 0.016 grams of 1PhPy was placed into individual 20 mL glass vials with each designated for a %volume ratio. Using a micropipette, 10 mL of the %volume solution was placed into each vial to dissolve the 1PhPy. The 20:80 sample was diluted to a concentration of approximately 0.00035 g/mL for full solvation. Fluorescence emission and excitation spectra were obtained using a Cary Eclipse Fluorescence Spectrophotometer (G9800A), whereby approximately 1 mL of the %volume sample solution was placed into a 1 cm quartz cuvette for analysis. Excitation spectra were obtained in the range of 190 nm to 325 nm with an emission wavelength of 330 nm, and emission spectra were obtained in the range of 285 nm to 800 nm with an excitation wavelength of 280 nm. The excitation and emission slit widths were 5 nm and the scan resolution was 1 nm. A series of 3 scans were taken for each sample and then averaged.

Computational Methods

Quantum Chemical Calculations.

All quantum chemical calculations were performed using the Gaussian16 suite.[32] The different conformers of 1PhPy were constructed by rotating the C-N dihedral bond between the pyrrole and phenyl aromatic rings shown in Figure 1. Ground-state vibrational frequency and optimization calculations were carried out using density functional theory (DFT), specifically the ωB97X-D level of theory with the 6-311G++(d,p) basis set.[33,34] The ωB97X-D functional has been used in previous studies considering its effectiveness at describing dispersive interactions between molecules as well as increasing long-range exact exchange, which removes long-range self-interactions. This allows for a more reliable modeling of charge transfer compared to other

functionals.[35] Analogous excited state calculations were carried out at the TD-DFT ωB97X-D/6-311++G(d,p) level of theory.

To search for the lowest-energy structures of the 1PhPy + nH_2O complexes, the ABCluster program[36] was employed to generate initial guess structures. The configurational search identifies global and local minima of molecular complexes using the artificial bee colony (ABC) algorithm, and all possible 1PhPy + nH_2O (n=1-3) complex isomers were obtained within a 50 kJ/mol energy window. Further geometry optimizations and harmonic frequency calculations were performed at the same levels of theory described for 1PhPy, and the lowest-energy isomers were identified. Vertical excitation calculations for 1PhPy and 1PhPy + nH_2O (n=1-3) were calculated for all optimized structures using TD-DFT ωB97XD/6-311++G(d,p). Relaxed potential energy scans along the C-N dihedral angle were generated for 1PhPy and 1PhPy + nH_2O (n=1-2) in the ground and excited states using the same levels of theory as the geometry optimization calculations. The 6-31G++(d,p) basis set was used for the 1PhPy + 3H_2O dihedral scan in the excited state due to computational costs. The dihedral angle was scanned in 10° increments, and the relative energies were recorded to predict barriers to planarity (ΔE_0) and perpendicularity (ΔE_{90}). Where necessary, the potential energy scans were also carried out at 5° and 1° increments to investigate any effects that the additional resolution would have on the potential energy fitting procedure.

Discrete Variable Simulation of the 1PhPy and 1PhPy+ H_2O Vibronic Spectra.

The vibronic spectra of 1PhPy and 1PhPy+ H_2O were simulated with periodic one-dimensional discrete variable representation (1D-DVR) calculations.[37] The formulation of the potential and kinetic energy matrices follow the methods of Colbert and Miller.[38] For the potential energy, torsional potential energy scans were fitted on the ground and excited states for both 1PhPy

and 1PhPy + 1H_2O. Two interpolation schemes were employed: cubic spline and linear interpolation, both constrained to periodic behavior. For the excited state of the 1PhPy molecule, the large and sudden jumps in the potential energy surface (see below) meant that a linear interpolation is a more robust fit. Thus, for consistency purposes, we employed a linear fit for all.

In the 1D-DVR calculations of the torsional energy levels and wavefunctions, 1001 grid points were used (2001 grid points were used to test for convergence). The relative intensities of transitions between ground state torsional wavefunctions found on each surface were taken to be the absolute value of the overlap integral (evaluated over the discrete grid points) between the two wavefunctions, and the intensities were normalized to the largest overlap. There were four empirical parameters that were added to finish fitting the spectra on top of this simplified model: 1) The position (in frequency) of the origin of the progression, 2) The effective mass of the torsion, 3) The starting point for the second progression with the same spacing (appears to be due to a second vibrational mode) 4) For the 1PhPy + 1H_2O spectrum, a cutoff for the spectral progression is set to 450 cm^{-1}. The relative intensity of the second progression is also a parameter that is tunable, in principle, but for this work was not employed. The DVR code and supplemental code for generating the estimated spectra are provided on GitHub: (https://github.com/Tabor-Research-Group/phenylpyrole-dvr).

Results

Computational Results

Figure 2 shows the optimized geometries for 1PhPy in the ground and excited electronic states. Only one conformer was found in the ground state with a CN-CC dihedral angle of 40.2°, which is a somewhat twisted configuration between complete planarity (0°) and complete

perpendicularity (90°). By comparison, two different minima were found in the excited state, in which the lowest-energy conformation has a dihedral angle of 67.9° that is closer to perpendicularity. Relative to the ground state geometry, the lowest-energy TICT isomer in the excited state has a bent structure with the pyrrole C-H bond oriented towards the phenyl ring. The NCC angle is 35°; here, we define the NCC angle as the difference between 180° and the angle between the pyrrole nitrogen atom and the phenyl ring carbon atoms at positions 1 and 4. The higher-energy locally-excited (LE) geometry with a dihedral angle = 23.3° and a NCC angle ~ 0° is less stable than the excited state global minimum by approximately 300 cm^{-1}. Both excited state geometries have previously been reported at the CASPT2//CASSCF level in the gas phase and in acetonitrile solution.[29] Tables 1 and 2 tabulate the geometrical parameters of 1PhPy in the ground and excited electronic states.

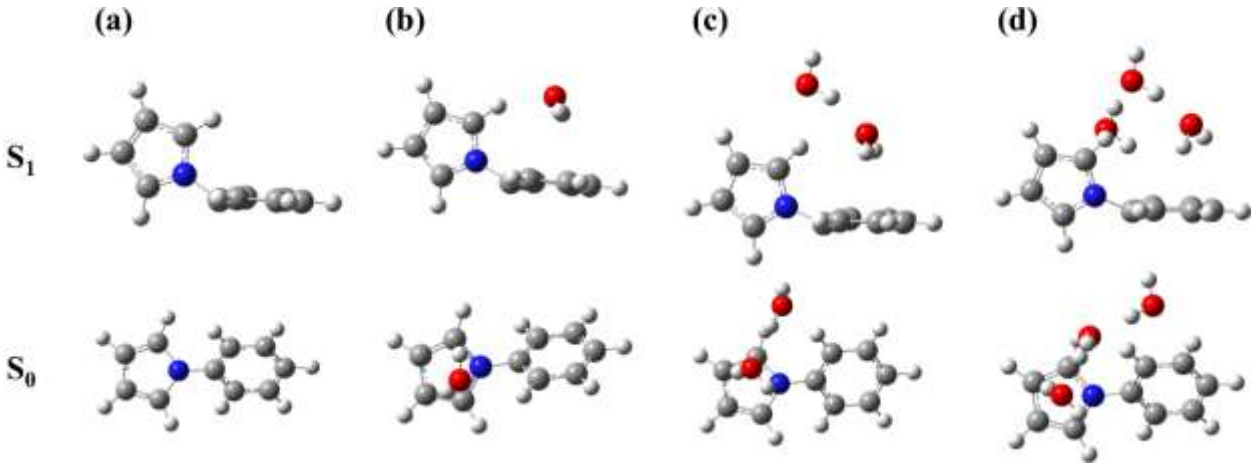

Figure 2: Optimized geometries of a) 1PhPy, b) 1PhPy + 1H_2O, c) 1PhPy + 2H_2O, and d) 1PhPy + 3H_2O in the ground (bottom) and excited (top) singlet electronic states at the ωB97X-D/6-311G++(d,p) and TD-DFT ωB97X-D/6-311G++(d,p) level of theory, respectively.

Table 1: Geometrical Parameters of the 1-Phenylpyrrole Optimized Structures With and Without Water in the Ground Electronic State[a]

	1PhPy	**1PhPy + 1H_2O**	**1PhPy + 2H_2O**	**1PhPy + 3H_2O**
Dihedral (˚)	40.2	-54.2	40.1	44.5
NCC Angle (˚)	0	0	0	1
N-C Bond Length (Å)	1.41	1.42	1.42	1.42

[a] Geometries optimized at the ωB97X-D/6-311G++(d,p) level.

Figure 2 also shows the calculated geometries in the ground and excited electronic states for the 1PhPy + 1H_2O, 1PhPy + 2H_2O, and 1PhPy + 3H_2O complexes; Tables 1 and 2 list the relevant parameters of 1PhPy + nH_2O in both electronic states. Upon excitation, the dihedral angles changes from a semi-twisted conformation in the ground state (-54.2°, 40.1°, and 44.5°) for 1PhPy + 1H_2O, 1PhPy + 2H_2O, and 1PhPy + 3H_2O, respectively, to a more perpendicular conformation in the excited state (70.3°, 74.1°, 91.2°). Furthermore, the NCC angle for 1PhPy + 1H_2O, 1PhPy + 2H_2O, and 1PhPy + 3H_2O, respectively, in the excited state is 29°, 25° and 23°. The excited state geometry of the 1PhPy solute within the water-complexed structures is similar to the bare 1PhPy chromophore such that the CH bond of the pyrrole ring orients towards the phenyl ring. Indeed, Figure 2 shows that 1PhPy adopts a bent structure upon excitation with a dihedral angle that increasingly approaches perpendicularity with the number of water molecules in the complex. A similar geometry of the 1PhPy chromophore in acetonitrile solvent has been reported in a previous theoretical study.[29] Calculations indicate that the $S_1 \leftarrow S_0$ adiabatic excitation energy decreases with sequential water addition relative to the bare 1PhPy chromophore and that the transition is consistent with a $\pi\pi^*$ excitation. Furthermore, higher-lying excited electronic states are not predicted to be close in energy to the first excited electronic state. As seen in the figure for 1PhPy + 1H_2O, water prefers to bind with the pyrrole ring in the ground electronic state through a

hydrogen atom-π interaction. However, upon excitation, this interaction changes with the water now bridging the two rings as both a hydrogen atom acceptor with the pyrrole ring and a donor to the π* orbital localized on the phenyl ring. The 1PhPy + nH_2O (n=2,3) complexes demonstrate similar ground and excited state interactions as the singly solvated complex, with the water network fully extending between the pyrrole and phenyl π-systems for 1PhPy + 3H_2O.

Table 2: Geometrical Parameters of the 1-Phenylpyrrole Optimized Structures With and Without Water in the First Excited Electronic State[a]

	1PhPy	**1PhPy + 1H_2O**	**1PhPy + 2H_2O**	**1PhPy + 3H_2O**
Dihedral (˚)	67.9	70.3	74.1	91.2
NCC Angle (˚)	35	29	25	23
N-C Bond Length (Å)	1.48	1.47	1.46	1.45

[a] Geometries optimized at the TD-DFT ωB97X-D/6-311G++(d,p) level.

As observed in the ground state dihedral potential energy scan shown in the bottom panel of Figure S1, 1PhPy has clear barriers to planarity (ΔE_0; dihedral angle=0°) and perpendicularity (ΔE_{90}; dihedral angle=90°) seen by the repetition of two transition state geometries. The calculated barriers ΔE_0 and ΔE_{90} are 652 cm^{-1} and 579 cm^{-1}, respectively. For the excited state dihedral scan shown in the upper panel of the figure, the global minimum geometry corresponds to a structure with a dihedral angle close to 90°, whereas the dihedral angle of the LE minimum geometry is near 0°. This torsional phase shift between the ground and excited electronic states leads to nuclear arrangements that may hinder or enhance electron charge transfer upon excitation as will be discussed in the Discussion section. Here, the lowest calculated barriers to interconversion are 863 cm^{-1} for the perpendicular conformation to isomerize to the planar configuration, whereas it would require 496 cm^{-1} for the planar structure to convert into the perpendicular geometry.

The ground state 1PhPy + 1H_2O potential energy scan is presented in Figure S2, showing different torsional barriers than 1PhPy. In particular for the ground state, ΔE_0 = 1033 cm^{-1}, whereas ΔE_{90} is significantly reduced to 174 cm^{-1}. The torsional potential energy surface for 1PhPy + 1H_2O in the excited state changes drastically compared to the bare 1PhPy chromophore. Strikingly, ΔE_0 = 2371 cm^{-1}, which is twice the energy than in the ground state, and there is no longer a barrier to perpendicularity. Similar figures displaying the torsional potential energy surfaces of 1PhPy + 2H_2O and 1PhPy + 3H_2O in both the ground and excited state can be found in the supplemental information (Figures S3 and S4). As will be discussed in the Discussion section, the addition of water significantly changes the preferred conformation, photophysics, and the degree to which intramolecular charge transfer occurs upon photoexcitation.

Experimental Results

The first 700 cm^{-1} of the resonant two-photon ionization (R2PI) spectrum for 1-phenylpyrrole (1PhPy) is shown in Figure 3. The electronic origin band located at 35490 cm^{-1} is similar to that reported by Okuyama and Thomas.[25,26] Upon closer inspection of the R2PI spectrum, a regular ~50 cm^{-1} spacing between vibronic transitions is built off the origin, in addition to further vibronic activity at higher energy. The vibronic peaks with ~50 cm^{-1} spacing is likely due to the torsion vibrational mode between the pyrrole and phenyl rings as observed in previous studies.[25,26] Okuyama et al. originally assigned alternating excited state vibronic bands with even quanta due to torsional transitions from v''=0 to v'=0, 2, 4, etc. (e.g., T_0^n, n=even), while also assigning odd number quanta to torsional transitions with v''=1 to v'=1, 3, 5, etc. (e.g., T_1^n, n=odd). More recently, the rotationally-resolved spectroscopy measurements recorded by Thomas et al. provided evidence that the torsional transitions originated from v''=0 since the rotational constants

remained the same for each transition. According to the calculated dihedral potential energy surface shown in Figure S1, the torsional barriers for 1PhPy are sufficiently large such that the low-lying torsional energy levels will occur in degenerate pairs. For example, the T_{0^+} and T_{0^-} levels are degenerate but have vibrational wave functions that are symmetric and antisymmetric, respectively, with respect to the planar configuration. The selection rules governing the observed vibronic transitions dictate that the vibrational wave function has the same symmetry with respect to torsion in both the ground and excited electronic states. Therefore, the label $T^n_{0^{+/-}}$ indicates the series of transitions $T^0_{0^+}$, $T^1_{0^-}$, $T^2_{0^+}$, $T^3_{0^-}$, etc.

We, therefore, reassign the peaks with a ~50 cm^{-1} spacing between adjacent vibronic bands to both even and odd quanta in the torsional mode ($T^n_{0^{+/-}}$) as originating from v''=0. Additionally, the 50 cm^{-1} torsional progression is in better agreement with the calculated torsional mode for the bent structure (T = 47 cm^{-1}) in the excited electronic state compared to the higher-energy LE isomer (T = 88 cm^{-1}). The vibronic peaks labeled blue in Figure 3 represent the progression with increasing quanta placed in the excited state torsional mode from v''=0, $T^n_{0^{+/-}}$. As predicted from calculations, the geometry change between the ground and excited electronic states is expected to be large, giving rise to a long Franck-Condon intensity profile.

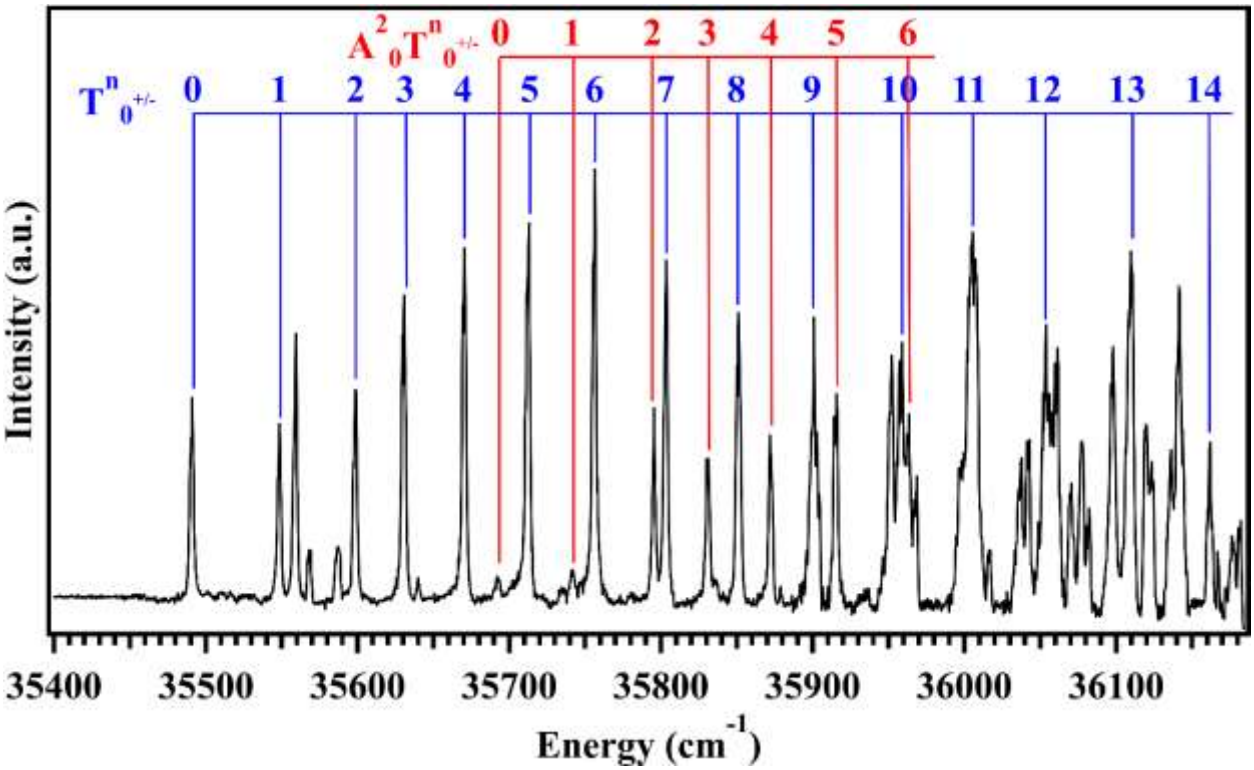

Figure 3: R2PI spectrum of 1-phenylpyrrole (1PhPy). The blue trace signifies transitions due to the torsional mode progression ($T^n_{0^{+/-}}$), and the red trace indicates the $A^2_0 T^n_{0^{+/-}}$ band progression with mixed vibrational mode character.

As previously mentioned, there is a significant change in geometry between the ground and excited electronic states of 1PhPy. Not only does the torsion dihedral shift, but the excited state calculations point to a geometry that is bent with the pyrrole ring oriented towards the phenyl ring. Therefore, vibrational modes reflecting this geometry change may plausibly be activated and observed in the electronic spectrum. The second progression labeled red in the R2PI spectrum in Figure 3 was mentioned in the work by Okuyama et al., but the authors did not make an assignment of the possible vibrational mode. We assign this progression (labeled $A^2_0 T^n_{0^{+/-}}$) to a combination band involving the torsional mode, $T^n_{0^{+/-}}$, with another type of nuclear motion since the spacing between vibronic peaks is approximately 50 cm^{-1}. The energy difference between the electronic origin band and the beginning of the $A^2_0 T^n_{0^{+/-}}$ progression is approximately 200 cm^{-1}. However,

there are no fundamental vibrational modes with frequencies that closely match this energy difference from theoretical calculations. Alternatively, there are two low-frequency modes shown in Figure 4 that are in good agreement with the onset of this progression when given two quanta. The *A* mode may belong to a twisting-like motion between the two aromatic rings (Figure 4) with a calculated frequency of 101 cm^{-1}. Here, this twisting-like vibrational mode has a″ symmetry in the C_s point group since its motion is perpendicular to symmetry plane. The overall symmetry of the vibronic wave functions must be totally symmetric to be observed in the R2PI spectrum, which is accomplished with an even number of quanta in the *A* vibrational mode. The observed transitions in the progression would then be $A_0^2T_{0^+}^0$, $A_0^2T_{0^-}^1$, $A_0^2T_{0^+}^2$, $A_0^2T_{0^-}^3$, etc. Another possible assignment of the $A_0^2T_{0^{+/-}}^n$ progression may involve the torsional mode combined with a bending-like motion between the pyrrole and phenyl rings shown in Figure 4, with a predicted frequency at 80 cm^{-1}. Activation of this vibrational mode is consistent with the large geometry change between the ground and excited electronic states, wherein the pyrrole ring is oriented towards the phenyl aromatic ring. With two quanta along this bending-like mode, the predicted vibronic band would be in close agreement with the observed beginning of the $A_0^2T_{0^{+/-}}^n$ progression. To obtain the correct overall symmetry, the progression would similarly be $A_0^2T_{0^+}^0$, $A_0^2T_{0^-}^1$, $A_0^2T_{0^+}^2$, $A_0^2T_{0^-}^3$, etc.

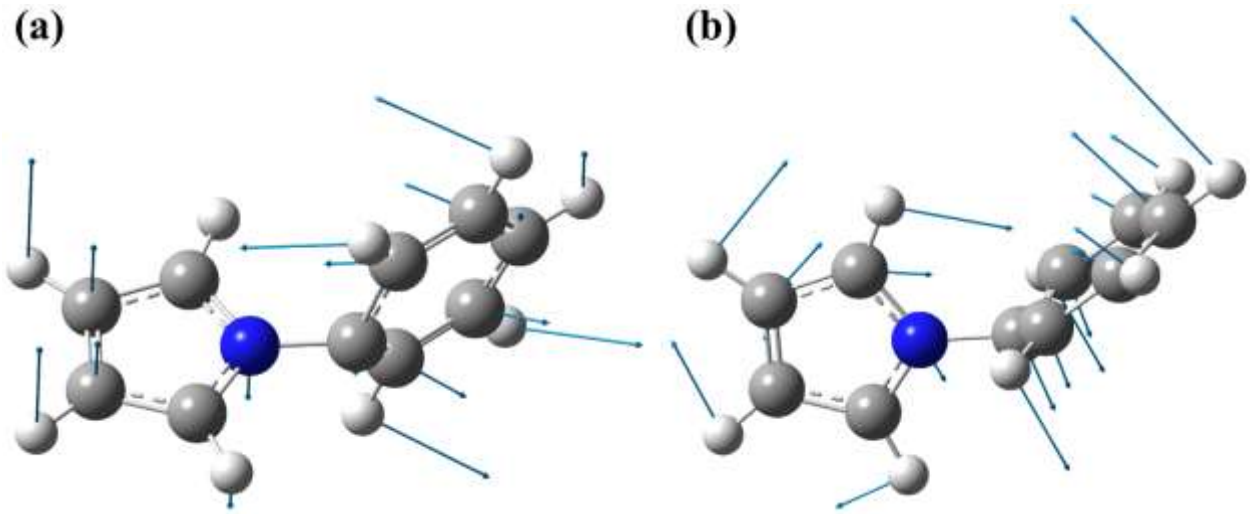

Figure 4: (a) Twisting-like and (b) bending vibrational modes of 1PhPy with arrows displaying the relative magnitudes of nuclear displacement. Calculations were performed at the TD-DFT ωB97X-D/6-311G++(d,p) level of theory.

Although ion signal was observed in the 1PhPy + $1H_2O$ mass channel, no resonant transitions were recorded when the probe wavelength was scanned. However, when water was entrained in the supersonic jet expansion, new transition bands were found in the R2PI spectrum of 1PhPy (top black trace in Figure 5) at longer wavelengths when monitoring the 1PhPy mass ion signal. We, therefore, used ultraviolet holeburning (UVHB) to separate and assign vibronic features due to individual isomers. The middle trace (labeled red) in the figure shows the holeburning spectrum due to 1PhPy when the holeburn laser is resonant on the transition in the R2PI spectrum labeled with a red asterisk. However, when the holeburn laser is resonant with the new vibronic peak labeled with a blue asterisk, we obtain the holeburning spectrum shown in the bottom of the figure (blue trace). Since there are no other predicted isomers of 1PhPy, we assign these new vibronic features to the 1PhPy + $1H_2O$ molecular complex decomposing to $1PhPy^+$ and water fragments following photoionization. The low-energy van der Waal's interaction (hydrogen atom-π) between 1PhPy and water is likely exceeded upon ionization of the molecular complex. We observe the same holeburning spectrum shown in the bottom of Figure 5 when the holeburn

laser is resonant with the other new bands not assigned to 1PhPy, albeit with a smaller signal-to-noise ratio. No ion signal in the mass spectrum could be observed for higher-order water complexes with 1PhPy that would indicate larger complexes decomposing into the $1PhPy^+$ mass channel; typical concentrations of water entrained in the gas expansion was ~0.05%. Furthermore, these new vibronic features disappear under warmer supersonic expansion conditions, indicating they are not due to 1PhPy 'hot bands'. The 1PhPy + $1H_2O$ vibronic spectrum is shown in Figure 6 with tentative assignments for the observed transitions. Similar to the bare 1PhPy chromophore, we observe regular spacing between the new vibronic transitions of approximately 70 cm^{-1}, which we assign to increasing quanta placed in the torsional mode, $T_{0^{+/-}}^{n}$.

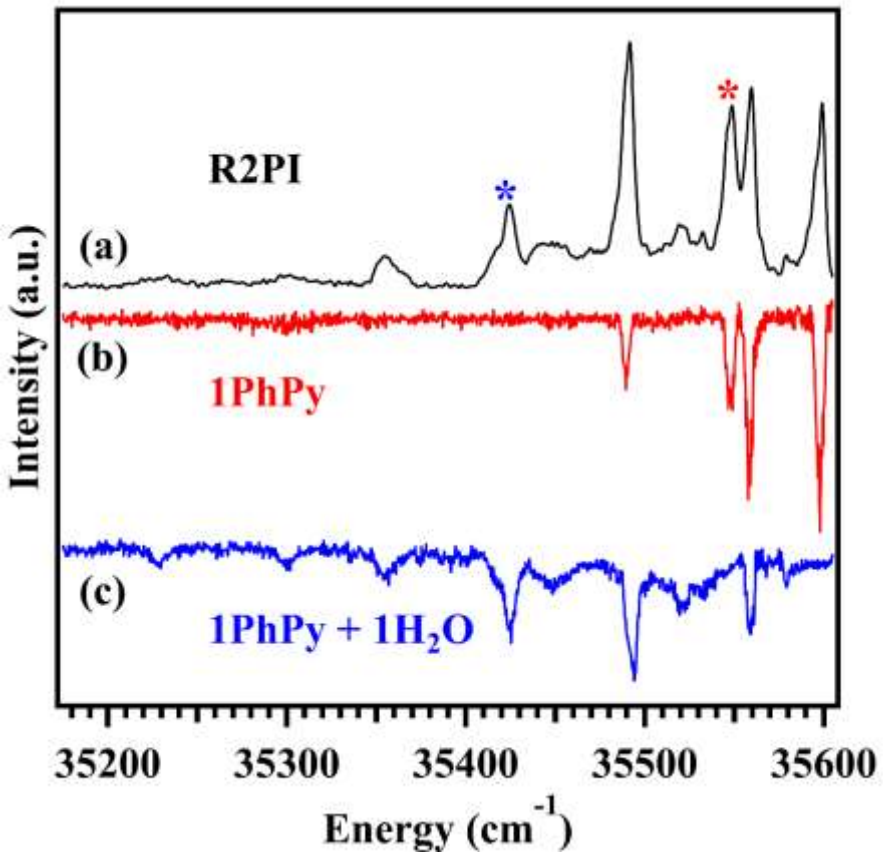

Figure 5: (top trace) R2PI spectrum recorded while monitoring the 1PhPy (m/z=143) mass channel when water is entrained in the gas expansion. (middle trace) Holeburn spectrum assigned to the bare 1PhPy chromophore obtained when the holeburn laser is resonant on the vibronic transition labeled with a red asterisk in the R2PI spectrum. (bottom trace) Holeburn spectrum assigned to the 1PhPy + $1H_2O$ complex when the holeburn laser is resonant on the new vibronic transition labeled with a blue asterisk in the R2PI spectrum.

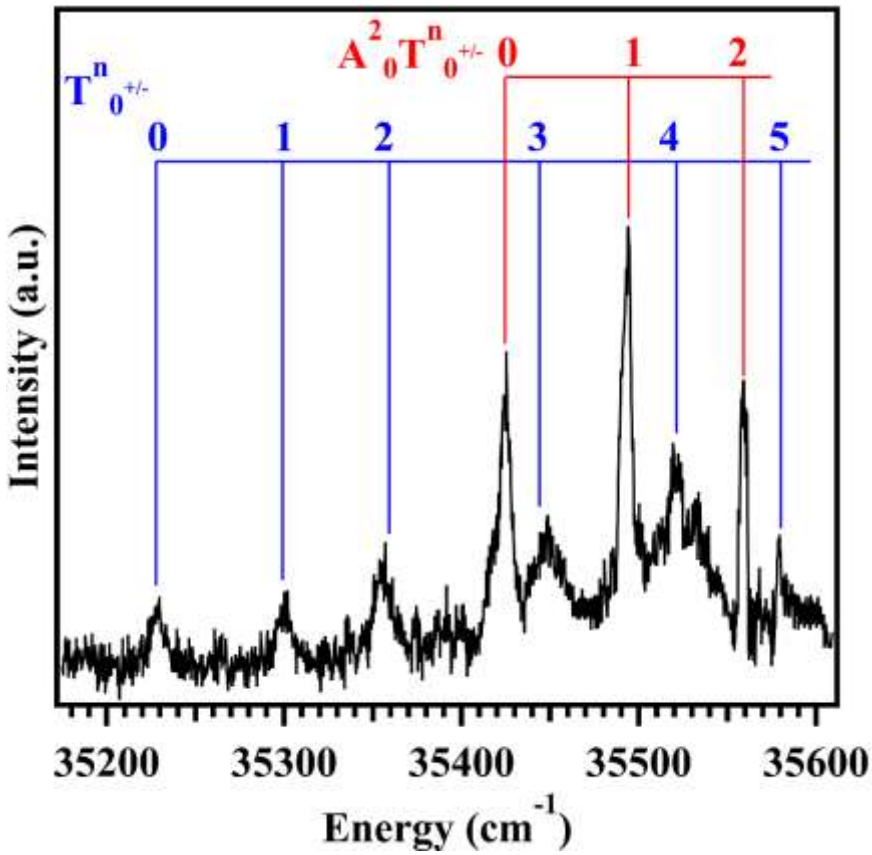

Figure 6: Vibronic spectrum of the 1PhPy + 1H_2O complex. The new vibronic features are assigned to the torsional modes $T^n_{0^{+/-}}$ (blue tie lines) and the $A^2_0T^n_{0^{+/-}}$ combination band (red tie lines) of 1PhPy + 1H_2O.

The electronic origin band is assigned to the lowest energy peak observed at 35227 cm^{-1}, which is red-shifted from the 1PhPy bare chromophore origin by 263 cm^{-1}. The intermolecular interaction of water with 1PhPy can be best described as a weak Coulombic attraction (water binds as a proton donor to the aromatic rings) rather than a true hydrogen bond. Thus, the relative stabilization of this interaction is reflected in the modest red-shift of the 1PhPy + 1H_2O electronic origin band with respect to 1PhPy. Additionally, the weak interaction between 1PhPy and water may also explain the likely fragmentation of the 1PhPy + 1H_2O complex upon photoionization, arising as new resonant features observed in the 1PhPy R2PI spectrum. The vibronic spectrum of 1PhPy + 1H_2O does not extend as far in energy with regards to the R2PI spectrum of 1PhPy, likely

due to the dissociation of the molecular complex to fragments. From the spectrum, we tentatively infer that the dissociation energy of 1PhPy + 1H_2O is approximately the energy difference between the electronic origin band and the last vibronic transition, ~ 350 cm^{-1}. We note that this value is lower than the calculated binding energy by about a factor of six (~2000 cm^{-1} depending on if zero-point effects are taken into account).

As shown in Figure 6, the 1PhPy + 1H_2O vibronic peaks have been assigned in a similar fashion as in the R2PI spectrum of 1PhPy. The transitions labeled blue in the figure have a spacing of approximately 70 cm^{-1}, which we assign to the torsional mode, $T_{0^{+/-}}^{n}$ having a calculated vibrational frequency of 74 cm^{-1} in the excited state. Shown in the upper panel of Figure S2, the 1PhPy + 1H_2O torsional potential energy surface in the excited state displays a barrier to planarity that is larger by a factor of two compared to the bare 1PhPy chromophore (Figure S1). We attribute the heightened barrier to the increased torsional mode frequency and therefore the observed torsional progression spacing in the 1PhPy + 1H_2O R2PI spectrum. Furthermore, the observed ~70 cm^{-1} progression is in excellent agreement with calculations predicting a torsional vibrational mode of 74 cm^{-1}.

Analogous to the 1PhPy R2PI spectrum, we assign the band at ~195 cm^{-1} above the electronic origin to the onset of the $A_0^2T_{0^{+/-}}^{n}$ progression. Here, the torsional mode and either the twisting or bending nuclear motions are also coupled; the nuclear motions of the twisting and bending modes of 1PhPy in the molecular complex are similar to the modes illustrated in Figure 4. For the 1PhPy + 1H_2O complex, the predicted frequency associated with the twisting motion is 114 cm^{-1}, which with two quanta would be in close agreement with the progression. Furthermore, the bending mode has a calculated vibrational frequency of 93 cm^{-1}, which would be predicted to lie close to the observed vibronic band. Symmetry concerns must also be considered. 1PhPy has a

clear plane of symmetry through the molecule with or without water complexation in the excited state, and therefore the same vibronic symmetry rules are expected to be similar, albeit somewhat more relaxed, to those described earlier for the bare 1PhPy chromophore.

Discussion

Simulation of Vibronic Spectra with 1D DVR calculations

The DVR calculations can be thought of as a more numerical approach to interpreting the spectra, which we can use to complement the interpretations and insights given above in the experimental section.

1PhPy + 1H_2O Spectrum

We begin our discussion with the 1PhPy + 1H_2O complex due to its simpler spectral structure. The fitted potential energy surfaces used in the DVR calculations (with energy levels in black) are shown in Figure 7a. The results for the fitted spectrum (described below) are shown in Figure 7b. Two models for the potential energy surface were considered: 1) the first model fits the torsional potential of the ground and the excited state to the electronic energy only (potential energy surface in Figure S2) and 2) the second model calculates the zero-point energy of the other vibrational modes. The second model, with ZPE, is used in Figure 7 (and 8 for 1PhPy). Zero-point-energy free spectra are provided in the supporting information (Figures S5) and show some minor changes due to the asymmetry that is induced by the zero-point energy. The energies and wavefunctions were calculated under the periodic formulation of the DVR method on both the ground and excited states.[38] Relative intensities are found from the absolute values of the overlap integrals from the ground state torsional wavefunctions and the excited state wavefunctions. The

ground state torsional potential has four lowest energy states within 20 cm^{-1} of each other, and all four are used as potential initial states when generating pairs of ground state potentials with the excited torsional states.

Though both the excited state and the ground state mass are in principle, tunable parameters, the spectrum is only sensitive to the excited state mass as the quartet of states on the ground state are close to each other (the fitted ground and excited masses are 72.1 amu and 69.1 amu, respectively).

As stated above, the addition of a considering transitions that involve a second vibrational mode is necessary to fully model the spectrum—this shift is set to 195 cm^{-1}, and the peaks that result from these transitions is shown in red. Peaks that result from purely torsional transitions are modeled in green. Making the first sharp peak the origin of a second transition fits better over the entire 35400 cm^{-1} to 35600 cm^{-1} range. The model contains a larger splitting between pairs of peaks than experimental observed, partially due to the potential having higher asymmetry, though spectral fits on a fully symmetrized potential (such as the electronic surface).

A closer look at the wavefunctions and energies of the numerical results can help with the interpretation of the spectrum. The ground state torsional surface has an alternating (high to low) structure in the barrier to rotation, which when plotted over one full period resembles a double-well of double-well structure. Since the lower barrier is still over 200 cm^{-1}, this potential structure or a torsional problem with such a high mass results in the ground state being nearly quadruply degenerate, as expected above. The excited state torsional surface only has two barriers every period, and this results in the states being nearly doubly degenerate pairs (within 14 cm^{-1} at low energy.

The largest overlaps between the torsional wavefunctions occur between the third torsional state on the ground state surface and the second torsional state on the excited state surface (a full list of the state overlaps in given in the supporting information as csv files). However, there are states with appreciable overlaps all the way up to the 40^{th} torsional state (which is calculated to be at ~1500 cm^{-1}). The spectrum would contain a much longer progression if the higher photoionization energies did not result in dissociation of the water molecule from 1PhPy.

One compromise that this implementation of the DVR approach has comes from the perspective of interpretability. The grid is defined on a semi-open interval (with the end point fixed at 360^{o}), but even at high numbers of grid points, there is an asymmetry on the end points. This leads to the final wavefunctions as calculated with the DVR method being localized to individual wells (for our non-uniform potentials), and thus, we do not obtain eigenstates states that map directly onto the 0^{-} and 0^{+} state interpretation given above.

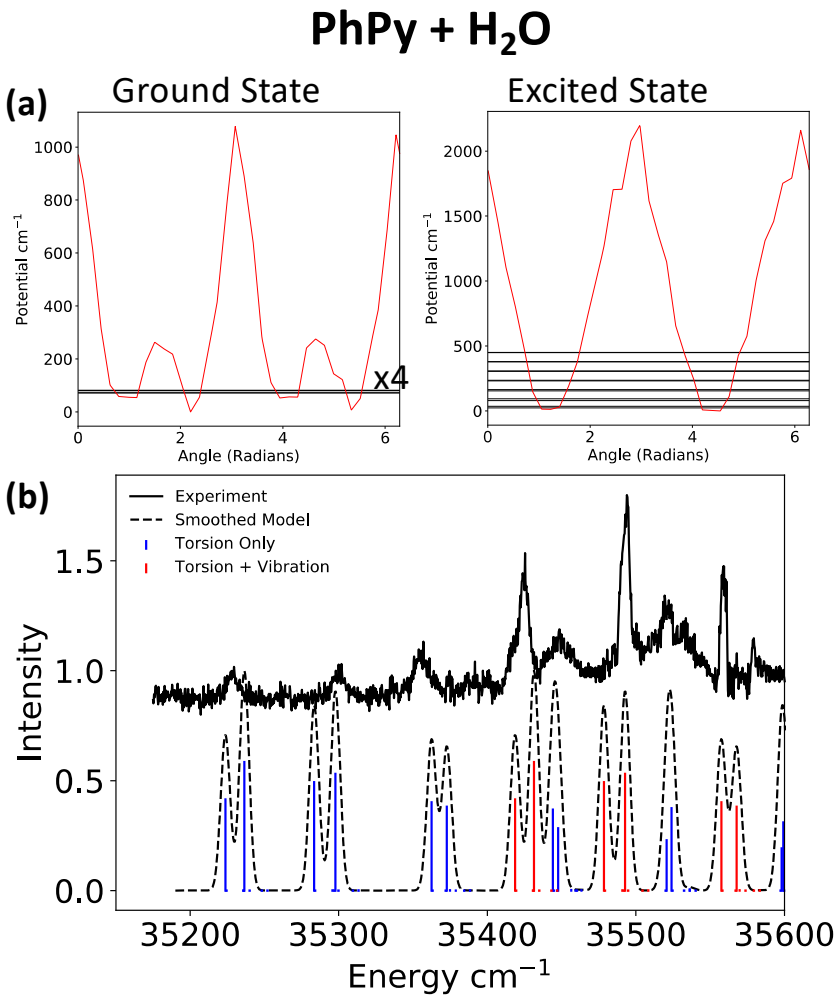

Figure 7: (a) Linear interpolated torsional potential energy surfaces for the 1PhPy + 1H_2O complex. The horizontal lines are the calculated energy levels from the 1D DVR calculations. The x4 on the ground state indicates that there are 4 states close to each other in energy. (b) Calculated spectrum for the 1PhPy + 1H_2O complex plotted against the experimental spectrum. Details provided in main text.

1PhPy Spectrum

The fitted ground and excited state surfaces of the model spectrum of 1PhPy are shown in Figure 8a and 8b, respectively. For this molecule, the simplified 1D-DVR picture is not able to capture all of the experimentally observed features. Specifically, the progression is predicted to continue to much higher energies than experimentally observed.

We again find a periodic double well of double-wells potential for the ground state, which results in the lowest four states forming a quartet on the ground state potential energy surface. The excited electronic state does not have pairs of torsional states until higher energy levels are reached. Unlike with the 1PhPy + 1H_2O complex, we do not have a reason to terminate the progression of the overlaps at lower energies. Thus, the spectrum under this simple one-dimensional model is expected to progress much longer than is experimentally observed. To understand these effects, it is likely necessary to account for dynamical effects or potentially higher-dimensional calculations would be needed. Despite these shortcomings, the approximate spacing and structure in the spectrum is reproducible through the same procedure employed in fitting the PhPy + 1H_2O spectrum. We note that the spectra fitted on the electronic-energy-only torsional potential (Figure S6) fits somewhat better at the lower frequency range.

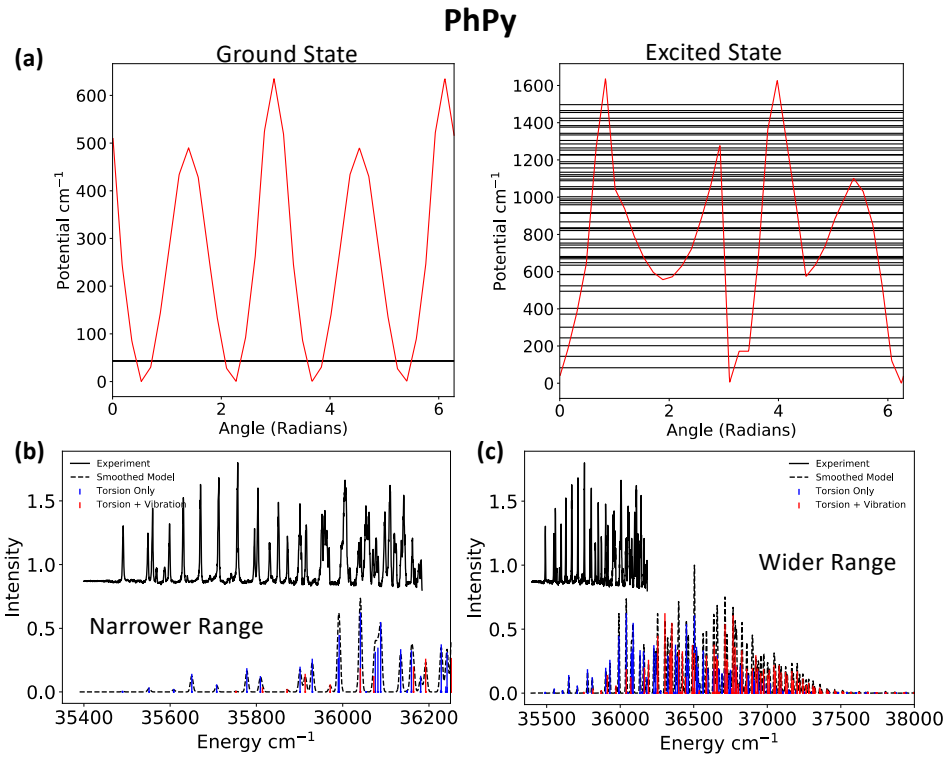

Figure 8: (a) Linear interpolated torsional potential energy surfaces and lower energy DVR energy levels for the 1PhPy molecule. (b&c) Calculated spectrum for the 1PhPy molecule plotted against the experimental spectrum, for narrower (b) and wider ranges (c), respectively.

Noncovalent Interactions Within Water-Solvated 1-Phenylpyrrole Complexes

To facilitate the interpretation of the intermolecular interactions present within the 1PhPy + nH_2O complexes, we performed a noncovalent interaction (NCI) analysis using NCIPLOT.[39] This method investigates the electron density regions, in which the reduced density gradient (RDG; $s(\rho)$) vanishes at low electron densities. The NCI analysis provides isosurfaces to visualize the RDG in regions far from the nuclei, where intermolecular interactions manifest themselves through singularities of the electron density. The sign of the second Hessian eigenvalue (λ_2) of the electronic density ρ distinguishes between different types of noncovalent interactions. The strength of the interaction can be derived from ρ in the corresponding region, which is color-coded with blue signifying strong hydrogen bonding, green representing weak van der Waals attraction, and red indicating strong repulsive interaction.

The 1PhPy geometries and extended hydrogen-bonding networks with water solvation shown in Figure 2 can be better understood by analyzing their respective intermolecular interactions. Figure 9 summarizes the NCI isosurfaces imprinted on the ground and excited electronic state geometries of 1PhPy + nH_2O, n=1-3. In general, water acts a reporter of the charge localization on the pyrrole or phenyl aromatic ring in the ground and excited electronic states. As can be seen in the figure, the water molecules have a propensity to interact with the pyrrole π orbital in the ground state, whereas water prefers to bind with the phenyl π^* orbital upon excitation of 1PhPy. In particular, the dominant interaction of the single water with 1PhPy in the ground state involves weak van der Waals attractions between the water hydrogen atoms with the pyrrole aromatic ring as indicated by the green isosurfaces. These weak interactions increase with two and three water molecules solvating 1PhPy, where the water network eventually bridges the pyrrole and phenyl rings for 1PhPy + 3H_2O with one water weakly attractive with the phenyl C-H bonds.

Furthermore, stronger hydrogen-bonding type interactions are observed between water molecules. As a result of the water hydrogen-bonding network accommodating 1PhPy via weak hydrogen/van der Waals interactions, the CN-CC dihedral of the 1PhPy solute in the molecular complexes changes appreciably from the bare 1PhPy chromophore.

Upon ππ* excitation of 1PhPy with the electron charge now localized on the phenyl ring, stabilization of the charge distribution is accomplished by a reorganization of the water hydrogen-bonding network. More specifically, the upper panel of Figure 9 illustrates water's key role in facilitating charge transfer between the pyrrole and phenyl aromatic rings. Indeed, the water network is increasingly stabilizing the nuclear geometry of the 1PhPy chromophore into a more perpendicular orientation. With the addition of a single water molecule, a weak attractive interaction is present between the water hydrogen atoms and the phenyl ring π* orbital, in addition to a stronger hydrogen bond between the oxygen atom of water and the pyrrole ring C-H bond. Therefore, the bent perpendicular geometry of 1PhPy within the complex is more stabilized compared with the bare 1PhPy chromophore. This geometrical change is also supported by the agreement of the DVR simulations of the complexed structure with the experimental observations. This is further demonstrated by the barrier to perpendicularity vanishing for the 1PhPy + 1H_2O excited electronic state shown in Figures 8 and S2. As the water network grows, the weak stabilizing attractions with the pyrrole ring steer the 1PhPy geometry towards a CN-CC dihedral angle approaching ~90°. Therefore, the NCI analysis reveals that upon sequential water molecule solvation of 1PhPy, the lower-energy twisted intramolecular charge transfer (TICT) geometry is obtained. The charge transfer dynamics and fluorescence emission outcomes of 1PhPy with an increasingly polar solvation environment are the focus of the next section.

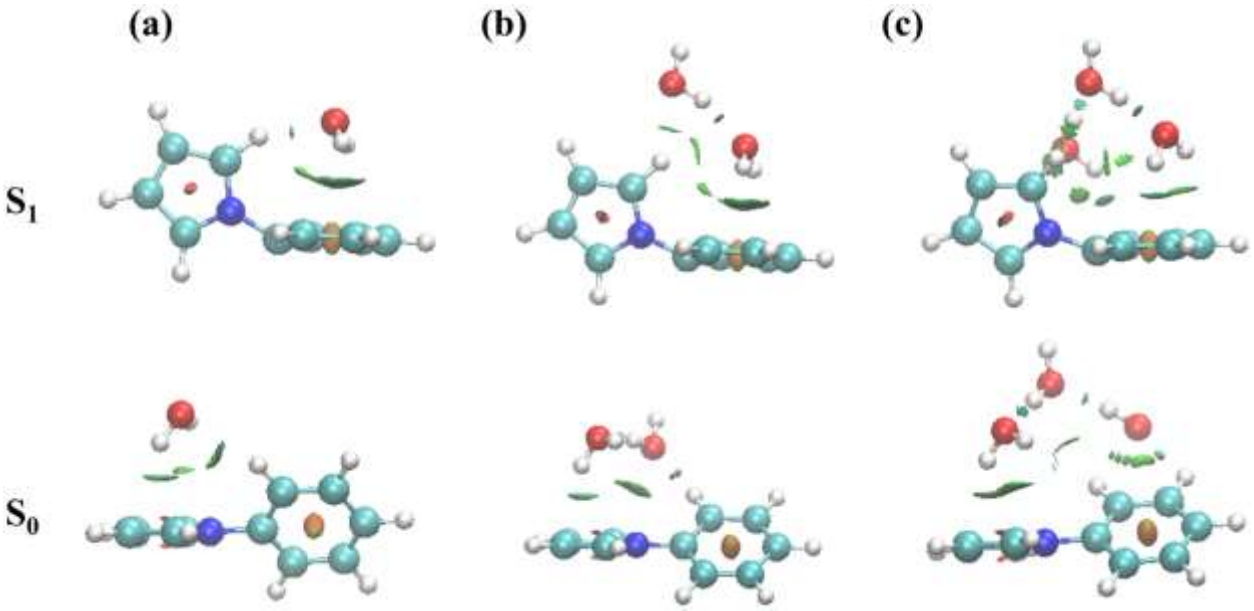

Figure 9: Noncovalent interactions and accompanying isosurfaces for both ground and excited states of (a) 1PhPy + 1H_2O, (b) 1PhPy + 2H_2O, and (c) 1PhPy + 3H_2O. Blue and green identify hydrogen bonding (strong attraction, blue) and van der Waals interactions (weak attraction, green). Red indicates repulsive interactions.

Twisted Intramolecular Charge Transfer Dynamics of 1-Phenylpyrrole

Visualizing the movement of charge that occurs when a molecular chromophore is excited is useful when understanding the TICT geometry of 1PhPy. To this end, calculations were carried out to obtain electron density difference maps for several dihedral angles of interest for the bare 1PhPy chromophore illustrated in Figure 10. Cyan indicates the areas of electron depletion within 1PhPy, while purple shows the areas of electron density gain upon excitation from the ground to excited electronic state. As shown in the figure, charge transfer appears to re-distribute from the pyrrole group to the phenyl ring in most conformations of 1PhPy, except when the dihedral angle approaches planarity which is at an energetic maximum. 1PhPy shows minimal charge transfer for the higher-energy isomer with a partially twisted geometry (47°) and for geometries possessing planar dihedral angles (0° or 180°). However, charge transfer from the pyrrole ring donor to the

phenyl ring acceptor is significant when 1PhPy adopts the lowest-energy bent configuration (TICT geometry) with a dihedral angle of 67.9°.

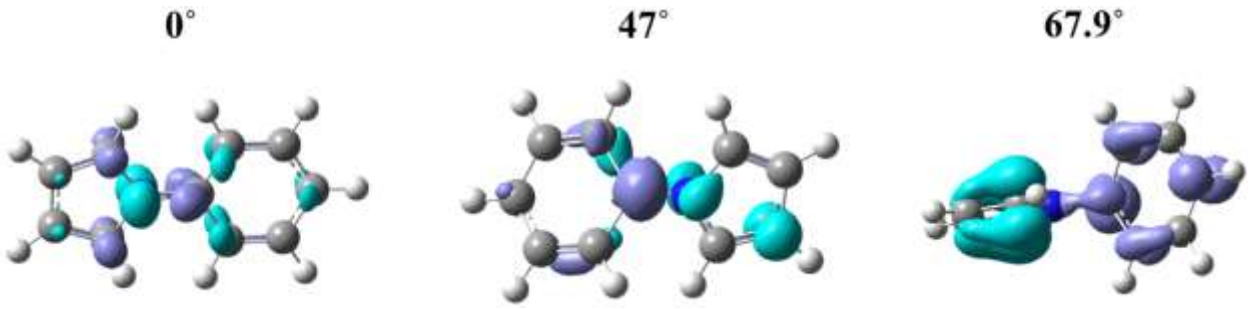

Figure 10: Electron density difference maps revealing the charge transfer for 1PhPy at different CN-CC dihedral angles in the excited electronic state. Cyan indicates the initial electron density in the HOMO and purple represents the final density shift to the LUMO after excitation.

Since solvent interactions are predicted to increase the likelihood of TICT in the previous literature, we expect different photophysical behavior for 1PhPy when it complexed with water.[27,40] As seen in Figure S2, the ground state barrier to perpendicularity (ΔE_{90}) is much lower for 1PhPy + 1H_2O than the 1PhPy bare chromophore. The ΔE_{90} difference is even more striking as revealed in the 1PhPy + 1H_2O excited state potential energy scan results. With the addition of a single water molecule, there is no ΔE_{90} for the 1PhPy + 1H_2O complex. In fact, the nearly perpendicular conformation is the lowest-energy geometry with barriers located at planarity (0° and 180°). The agreement between the R2PI spectrum and the DVR simulations for 1PhPy + 1H_2O further indicates a substantial decrease in energy for ΔE_{90}, supporting that TICT is enhanced with water solvation. Close inspection of the 1PhPy + 1H_2O electron density difference maps in Figure 11 show that charge transfer is evident at all the dihedral angle conformations, particularly when the 1PhPy chromophore in the complex resembles the bent TICT geometry with a CN-CC dihedral angle closer to 90°. These results indicate that water solvent intermolecular interactions are extremely important in facilitating the TICT configuration for 1PhPy.

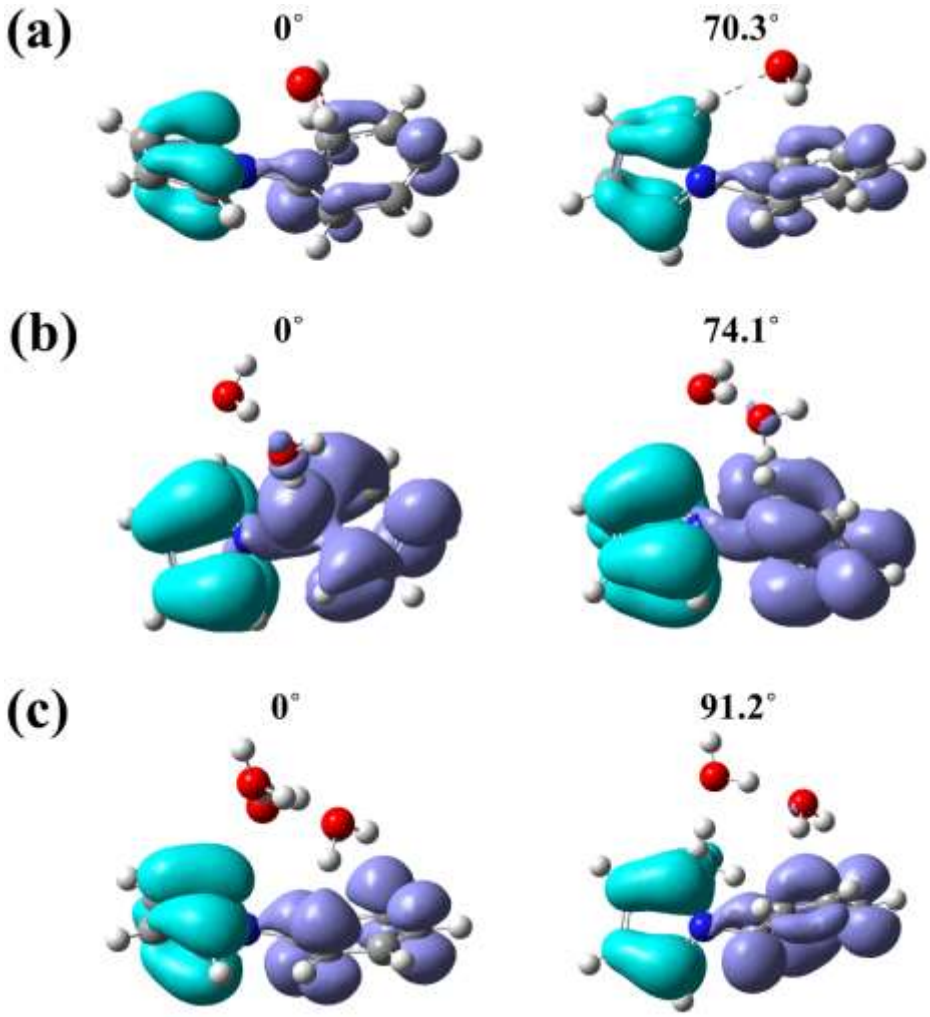

Figure 11: Electron density difference maps revealing the charge transfer for (a) 1PhPy + 1H_2O, (b) 1PhPy + 2H_2O, and (c) 1PhPy + 3H_2O at different CN-CC dihedral angles in the excited electronic state. Cyan indicates the initial electron density in the HOMO and purple represents the final density shift to the LUMO after excitation.

To further explore the importance of water solvation in facilitating TICT in 1PhPy, we carried out analogous calculations for 1PhPy + nH_2O (n=2, 3). Figure 11 also shows that charge transfer occurs for 1PhPy + 2H_2O at all dihedral angles, even for planar and perpendicular geometries. Additionally, 1PhPy + 3H_2O continues this trend, where conformations with CN-CC dihedral angles at 0°, 90° and 180° show charge transfer is facilitated by the water solvation network. This result is reflected in the dihedral potential energy surfaces (see Figures S3 and S4

in supporting information), where a more perpendicular TICT geometry is also the lowest-energy excited state conformation for 1PhPy + nH_2O (n=2,3).

As observed from the electron density difference map results, the polar water solvation environment stabilizes the excited state TICT geometry, acquiring an increasingly perpendicular CN-CC dihedral and less strained NCC angle with the size of the hydrogen-bonding network. Previous theoretical and experimental studies on the fluorescence of 1PhPy in different nonpolar and polar solvents have demonstrated dual emission bands.[23,24,29] These studies rationalized the red-shifted emission feature appearing in acetonitrile as a signature of 1PhPy undergoing torsional isomerization from the locally-excited (LE) electronic state configuration to the more stabilized TICT geometry. Radiative relaxation from the excited state TICT configuration to the ground electronic state is therefore often referred to as the charge transfer emission band and is observed at lower fluorescence energy.

To connect our gas-phase 1PhPy + nH_2O complex studies to the water-aqueous environment surrounding brown carbon (BrC) chromophores within aerosols, we obtained the absorption and fluorescence spectra of 1PhPy in nonpolar tetrahydrofuran (THF) solvent with an increasing % volume of water. Figure 12 shows the absorption spectrum (black trace) of 1PhPy in 100% volume THF. Using 280 nm (35714 cm^{-1}) as the excitation wavelength, we obtained the corresponding fluorescence spectrum in 100% volume THF showing a single emission band at ~32000 cm^{-1} resulting from the LE state in relatively nonpolar solvents. As greater % volume H_2O is incorporated into the samples, the appearance of the second TICT emission band is observed at approximately 25000 cm^{-1} with a concomitant decrease in intensity of the LE band. Therefore, with increasingly polar water solvation environments surrounding 1PhPy chromophores, the results indicate that emission from the excited state TICT geometry becomes dominant for larger

concentrations of water. This is consistent with the 1PhPy + nH_2O results, wherein water directly facilitates a TICT geometry from which the signature emission band is observed at lower energy in the fluorescence spectra. Aguilar and co-workers[29] reported the optimized geometries and energetics in the ground, LE and TICT electronic states in the gas phase and in acetonitrile solution. 1PhPy adopted a preferred TICT geometry in acetonitrile, wherein emission to the ground state explained the charge transfer emission band in polar solvents. They concluded that the TICT state is stabilized, and its energy becomes similar to the LE minimum. Therefore, the dual fluorescence was attributed to the TICT geometry accessible in polar solvents due to the free energy surface being very flat, making emission possible from any point along the path from the LE state to the TICT state.

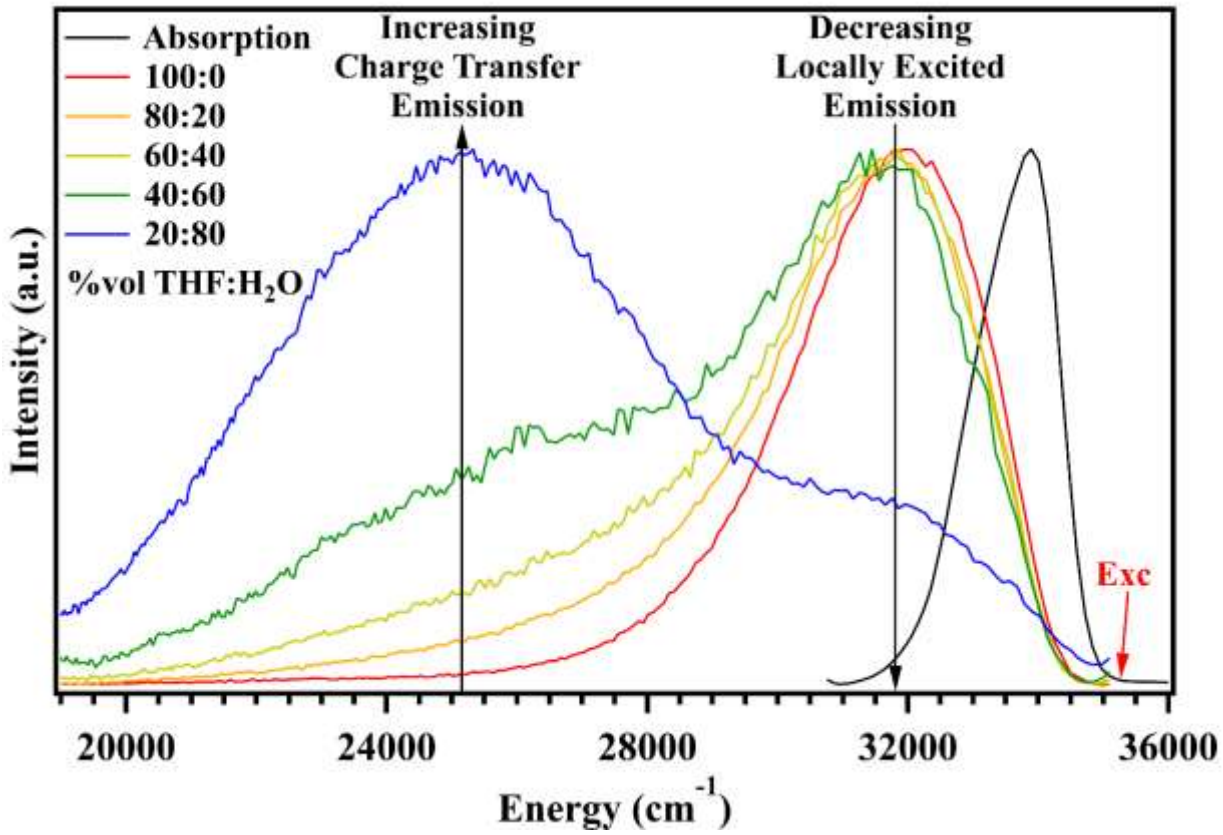

Figure 12: Absorption and fluorescence spectra of 1-phenylpyrrole in tetrahydrofuran (THF) with increasing %volume of water (H_2O) at 25°C. In 100% volume THF, the fluorescence spectrum consists of an emission from a locally-excited (LE) state. As the %volume H_2O increases, the fluorescence spectra display decreasing relative emission intensity from the LE state and increasing emission from the twisted intramolecular charge transfer (TICT) state. The excitation wavelength used during experiments was 280 nm.

Conclusions

To develop a better understanding of the photophysics of a prototypical chromophore in brown carbon (BrC) aerosols, we explore the local solvation intermolecular interactions of 1PhPy with H_2O. The present study on 1PhPy + nH_2O clusters (n=0-3) have provided a molecular-scale picture of the charge transfer dynamics of 1PhPy with and without the presence of water. Using a combination of experimental and theoretical approaches, we determined that H_2O plays an active role in facilitating the structural orientation and thus the charge transfer efficacy of 1PhPy.

Spectroscopic assignments for 1PhPy and 1PhPy + 1H_2O have been made using mass-resolved double-resonance spectroscopies and interpreted using 1-dimensional discrete variable representation (1D-DVR) simulations. Progressions in the torsional mode ($T^n_{0^{+/-}}$) are observed in the excited state spectra of 1PhPy and 1PhPy + 1H_2O, in which the spacings between transitions are ~50 and 70 cm^{-1}, respectively. Furthermore, either the bending or twisting-like nuclear motions couple with the torsional mode, yielding the other $A^2_0T^n_{0^{+/-}}$ progression. Indeed, the spectroscopy reveals that the intermolecular interactions with H_2O result in 1PhPy preferring a twisted intramolecular charge transfer (TICT) geometry. The sequential binding of H_2O to 1PhPy stabilizes the TICT geometry with a CN-CC dihedral that is nearly perpendicular, facilitating charge transfer from the pyrrole π orbital donor to the phenyl π* orbital acceptor. Predictions from analysis of the noncovalent interactions and electron density different maps upon photoexcitation indicate that the local H_2O environment mediates the charge transfer within 1PhPy by reorganizing the hydrogen bonding network. Measurements from condensed-phase experiments agree with the gas-phase results, whereby we observe greater fluorescence emission from the TICT geometry of 1PhPy as the concentration of H_2O is increased.

Acknowledgements

This material is based upon work supported by the National Science Foundation to NMK under Grant No. CHE-2102501. Partial support of this research from the Commonwealth Center for Energy and the Environment is also gratefully acknowledged by BNP, MEA, DJH, CDH, DVC and NMK. NMK also acknowledges William & Mary Research Computing for providing computational resources that contributed to the results reported within this paper. DPT acknowledges support from Texas A&M University startup funding and the Robert A. Welch Foundation (Grant No. A-2049-20200401). Portions of this research were conducted with high-performance research computing resources provided by Texas A&M University HPRC.

References

(1) Xantheas, S. S.; Voth, G. A. Aqueous Solutions and Their Interfaces. *J. Phys. Chem. B* **2009**, *113*, 3997–3999.

(2) Rodgers, J. M.; Weeks, J. D. Interplay of Local Hydrogen-Bonding and Long Ranged Dipolar Forces in Simulations of Confined Water. *Proc. Nat. Acad. Sci. U.S.A.* **2008**, *105*, 19136–19141.

(3) Cheung, M. S.; Garcia, A. E.; Onuchic, J. N. Protein Folding Mediated by Solvation: Water Expulsion and Formation of the Hydrophobic Core Occur After the Structural Collapse. *Proc Nat Acad Sci USA* **2002**, *99*, 685–690.

(4) Zhuravlev, P. I.; Papoian, G. A. Functional Versus Folding Landscapes: The Same Yet Different. *Curr. Opin. Struct. Biol.* **2010**, *20*, 16–22.

(5) Onuchic, J. N.; Wolynes, P. G. Theory of Protein Folding. *Curr. Opin. Struct. Biol.* **2004**, *14*, 70–75.

(6) Hoff, A. J.; Deisenhofer, J. Photophysics of Photosynthesis. Structure and Spectroscopy of Reaction Centers of Purple Bacteria. *Phys. Rep.* **1997**, *287*, 2–247.

(7) Magnuson, A.; Anderlund, M.; Johansson, O.; Lindblad, P.; Lomoth, R.; Polivka, T.; Ott, S.; Stensjo, K.; Styring, S.; Sundstrom, V.; Hammarstrom, L. Biomimetic and Microbial Approaches to Solar Fuel Generation. *Acc. Chem. Res.* **2009**, *42*, 1899–1909.

(8) LeBard, D. N.; Matyushov, D. V. Energetics of Bacterial Photosynthesis. *J. Phys. Chem. B* **2009**, *113*, 12424–12437.

(9) Bianchi, F.; Tröstl, J.; Junninen, H.; Frege, C.; Henne, S.; Hoyle, C. R.; al., et. New Particle Formation in the Free Troposphere: A Question of Chemistry and Timing. *Science (80-.).* **2016**, *352*, 1109–1112.

(10) Bzdek, B. R.; DePalma, J. W.; Johnston, M. V. Mechanisms of Atmospherically Relevant Cluster Growth. *Acc. Chem. Res.* **2017**, *50* (8), 1965–1975. https://doi.org/10.1021/acs.accounts.7b00213.

(11) Bzdek, B. R.; Reid, J. P. Aerosol Microphysics: From Molecules to the Chemical Physics of Aerosols. *J. Chem. Phys.* **2017**, *147*, 220901.

(12) Tabor, D. P.; Kusaka, R.; Walsh, P. S.; Sibert, E. L.; Zwier, T. S. Isomer-Specific Spectroscopy of Benzene-(H2O) n, n = 6,7: Benzene's Role in Reshaping Water's Three-Dimensional Networks. *J. Phys. Chem. Lett.* **2015**, *6* (10), 1989–1995. https://doi.org/10.1021/ACS.JPCLETT.5B00786/SUPPL_FILE/JZ5B00786_SI_001.PDF.

(13) Headrick, J. M.; Diken, E. G.; Walters, R. S.; Hammer, N. I.; Christie, R. A.; Cui, J.; Myshakin, E. M.; Duncan, M. A.; Johnson, M. A.; Jordan, K. D. Chemistry: Spectral Signatures of Hydrated Proton Vibrations in Water Clusters. *Science (80-.).* **2005**, *308* (5729), 1765–1769. https://doi.org/10.1126/SCIENCE.1113094/ASSET/72EB6CFC-FDB0-48E1-80E3-518C44E36C06/ASSETS/GRAPHIC/308_1765_F3.JPEG.

(14) Pachauri, R. K.; Meyer, L. A. Climate Change 2014: Synthesis Report. Contribution of Working Groups I, II and III to the Fifth Assessment Report of the Intergovernmental Panel on Climate Change. Geneva, Switzerland.

(15) Lary, D. J.; Lee, A. M.; Toumi, R.; Newchurch, M. J.; Pirre, M.; Renard, J. B. Carbon Aerosols and Atmospheric Photochemistry. *J. Geophys. Res. Atmos.* **1997**, *102* (D3), 3671–3682. https://doi.org/10.1029/96JD02969.

(16) Chung, S. H.; Seinfeld, J. H. Global Distribution and Climate Forcing of Carbonaceous Aerosols. *J. Geophys. Res. Atmos.* **2002**, *107* (D19), AAC 14-1.

https://doi.org/10.1029/2001JD001397.
(17) Andreae, M. O.; Gelencsér, A. Black Carbon or Brown Carbon? The Nature of Light-Absorbing Carbonaceous Aerosols. *Atmos. Chem. Phys.* **2006**, *6* (10), 3131–3148. https://doi.org/10.5194/ACP-6-3131-2006.
(18) Carslaw, K. S.; Lee, L. A.; Reddington, C. L.; Pringle, K. J.; Rap, A.; Forster, P. M.; Mann, G. W.; Spracklen, D. V; Woodhouse, M. T.; Regayre, L. A.; Pierce, J. R. Large Contribution of Natural Aerosols to Uncertainty in Indirect Forcing. *Nature* **2013**, *503*, 67–71.
(19) McCoy, I. L.; McCoy, D. T.; Wood, R.; Regayre, L. A.; Watson-Parris, D.; Grosvenor, D. P.; Mulcahy, J. P.; Hu, Y.; Bender, F. A. M.; Field, P. R.; Carslaw, K. S.; Gordon, H. The Hemispheric Contrast in Cloud Microphysical Properties Constrains Aerosol Forcing. *Proc. Nat. Acad. Sci. USA* **2020**, *117*, 18998–19006.
(20) Lin, G.; Penner, J. E.; Flanner, M. G.; Sillman, S.; Xu, L.; Zhou, C. Radiative Forcing of Organic Aerosol in the Atmosphere and on Snow: Effects of SOA and Brown Carbon. *J. Geophys. Res. Atmos.* **2014**, *119* (12), 7453–7476. https://doi.org/10.1002/2013JD021186.
(21) Laskin, A.; Laskin, J.; Nizkorodov, S. A. Chemistry of Atmospheric Brown Carbon. *Chem. Rev.* **2015**, *115*, 4335–4382.
(22) Phillips, S. M.; Smith, G. D. Light Absorption by Charge Transfer Complexes in Brown Carbon Aerosols. *Environ. Sci. Technol. Lett.* **2014**, *1* (10), 382–386. https://doi.org/10.1021/EZ500263J.
(23) Yoshihara, T.; Druzhinin, S. I.; Zachariasse, K. A. Fast Intramolecular Charge Transfer with a Planar Rigidized Electron Donor/Acceptor Molecule. *J. Am. Chem. Soc.* **2004**, *126* (27), 8535–8539. https://doi.org/10.1021/JA049809S.
(24) Yoshihara, T.; Druzhinin, S. I.; Demeter, A.; Kocher, N.; Stalke, D.; Zachariasse, K. A. Kinetics of Intramolecular Charge Transfer with N-Phenylpyrrole in Alkyl Cyanides. *J. Phys. Chem. A* **2005**, *109* (8), 1497–1509. https://doi.org/10.1021/JP046586J/SUPPL_FILE/JP046586J_S.PDF.
(25) Okuyama, K.; Numata, Y.; Odawara, S.; Suzuka, I. Electronic Spectra of Jet-Cooled 1-Phenylpyrrole: Large-Amplitude Torsional Motion and Twisted Intramolecular Charge-Transfer Phenomenon. *J. Chem. Phys.* **1998**, *109* (17), 7185. https://doi.org/10.1063/1.477355.
(26) Thomas, J. A.; Young, J. W.; Fleisher, A. J.; Alvarez-Valtierra, L.; Pratt, D. W. Stark-Effect Studies of 1-Phenylpyrrole in the Gas Phase. Dipole Reversal upon Electronic Excitation. *J. Phys. Chem. Lett.* **2010**, *1* (13), 2017–2019. https://doi.org/10.1021/JZ100653J.
(27) Proppe†, B.; Manuela Merchán*, ‡; Serrano-Andrés§, L. Theoretical Study of the Twisted Intramolecular Charge Transfer in 1-Phenylpyrrole. *J. Phys. Chem. A* **2000**, *104* (7), 1608–1616. https://doi.org/10.1021/JP993627G.
(28) Manz, J.; Proppe, B.; Schmidt, B. Time-Resolved Dual Fluorescence of 1-Phenylpyrrole in Acetonitrile: Molecular Dynamics Simulations of Solvent Response to Twisted Intramolecular Charge Transfer. *Phys. Chem. Chem. Phys.* **2002**, *4* (10), 1876–1881. https://doi.org/10.1039/B109488B.
(29) Galván, I. F.; Martín, M. E.; Muñoz-Losa, A.; Sánchez, M. L.; Aguilar, M. A. Solvent Effects on the Structure and Spectroscopy of the Emitting States of 1-Phenylpyrrole. *J. Chem. Theory Comput.* **2011**, *7* (6), 1850–1857. https://doi.org/10.1021/CT2001182.
(30) Schweke, D.; Haas, Y.; Dick, B. Photophysics of Phenylpyrrole Derivatives and Their

Acetonitrile Clusters in the Gas Phase and in Argon Matrixes: Simulations of Structure and Reactivity. *J. Phys. Chem. A* **2005**, *109* (17), 3830–3842. https://doi.org/10.1021/JP0500844.

(31) Pan, C.; Zhang, Y.; Lee, J. D.; Kidwell, N. M. Imaging the Dynamics of CH2BrI Photodissociation in the Near Ultraviolet Region. *J. Phys. Chem. A* **2018**, *122* (15), 3728–3734. https://doi.org/10.1021/acs.jpca.7b12268.

(32) Frisch, M. J., Trucks, G. W., Schlegel, G. W., Scuseria, G. E., Robb, M. A., Cheeseman, J. R., Scalmani, G., Barone, V., Petersson, G. A., Nakatsuji, H., Li, X., Caricato, M., Marenich, A. V., Bloino, J., Janesko, B. G., Gomperts, R., Mennucci, B., Hratch, H. P. Gaussian 16, Revision C.01.

(33) Chai, J. D.; Head-Gordon, M. Long-Range Corrected Hybrid Density Functionals with Damped Atom-Atom Dispersion Corrections. *Phys. Chem. Chem. Phys.* **2008**, *10*, 6615–6620.

(34) Chai, J. D.; Head-Gordon, M. Systematic Optimization of Long-Range Corrected Hybrid Density Functionals. *J. Chem. Phys.* **2008**, *128*, 84106.

(35) Rohrdanz, M. A.; Martins, K. M.; Herbert, J. M. A Long-Range-Corrected Density Functional That Performs Well for Both Ground-State Properties and Time-Dependent Density Functional Theory Excitation Energies, Including Charge-Transfer Excited States. *J. Chem. Phys.* **2009**, *130* (5), 054112. https://doi.org/10.1063/1.3073302.

(36) Zhang, J.; Dolg, M. ABCluster: The Artificial Bee Colony Algorithm for Cluster Global Optimization. *Phys. Chem. Chem. Phys.* **2015**, *17* (37), 24173–24181. https://doi.org/10.1039/C5CP04060D.

(37) Korn, J. A.; Tabor, D. P.; Sibert, E. L.; Zwier, T. S. Conformation-Specific Spectroscopy of Alkyl Benzyl Radicals: Effects of a Radical Center on the CH Stretch Infrared Spectrum of an Alkyl Chain. *J. Chem. Phys.* **2016**, *145* (12), 124314. https://doi.org/10.1063/1.4963227.

(38) Colbert, D. T.; Miller, W. H. A Novel Discrete Variable Representation for Quantum Mechanical Reactive Scattering via the S-matrix Kohn Method. *J. Chem. Phys.* **1998**, *96* (3), 1982. https://doi.org/10.1063/1.462100.

(39) Contreras-García, J.; Johnson, E. R.; Keinan, S.; Chaudret, R.; Piquemal, J.-P.; Beratan, D. N.; Yang, W. NCIPLOT: A Program for Plotting Noncovalent Interaction Regions. *J. Chem. Theory Comput.* **2011**, *7* (3), 625–632. https://doi.org/10.1021/CT100641A.

(40) Sasaki, S.; Drummen, G. P. C.; Konishi, G. Recent Advances in Twisted Intramolecular Charge Transfer (TICT) Fluorescence and Related Phenomena in Materials Chemistry. *J. Mater. Chem. C* **2016**, *4* (14), 2731–2743. https://doi.org/10.1039/C5TC03933A.

Supplementary Information to: Solvent-Mediated Charge Transfer Dynamics of a Model Brown Carbon Aerosol Chromophore: Photophysics of 1-Phenylpyrrole Induced by Water Solvation

Brianna N. Peterson,[1] Megan E. Alfieri,[1] David J. Hood,[1] Christian D. Hettwer,[1] Daniel V. Costantino,[1] Daniel P. Tabor,[2,a] Nathanael M. Kidwell[1,a]

[1] *Department of Chemistry, The College of William and Mary, Williamsburg, VA 23187-8795, USA*

[2] *Department of Chemistry, Texas A&M University, College Station, TX 77843, USA*

Contents:

Electronic Torsional Potential Energy Surfaces

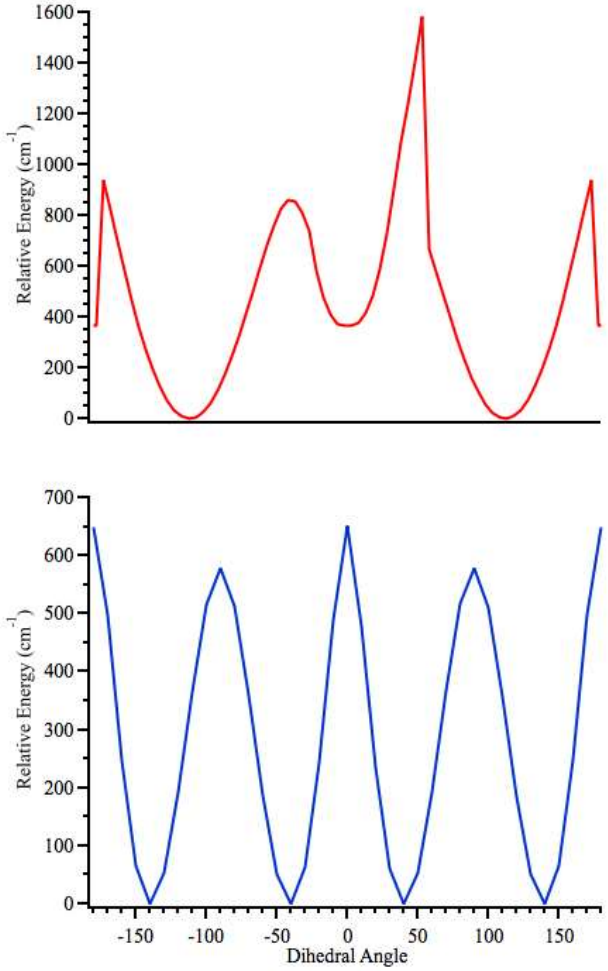

Figure S1: Potential energy surfaces (electronic energy only) of 1PhPy in the ground (lower panel) and excited electronic states (upper panel).

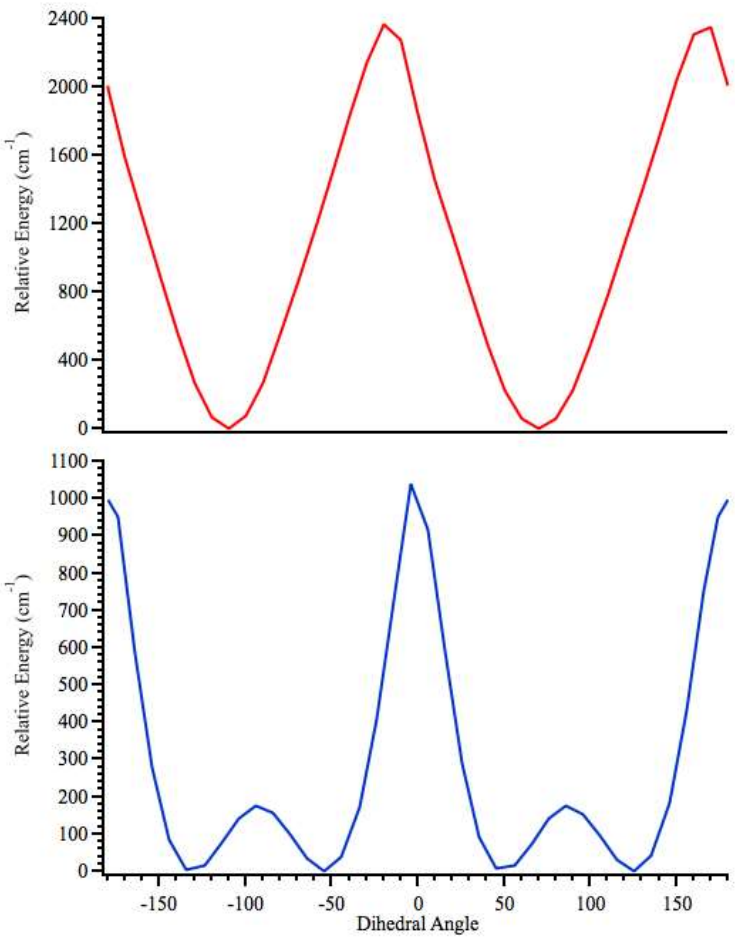

Figure S2: Potential energy surfaces (electronic energy only) of 1PhPy + 1H_2O in the ground (lower panel) and excited electronic states (upper panel).

1PhPy + 2H_2O and 1PhPy + 3H_2O Electronic Potential Energy Surfaces

For the 1PhPy + 2H_2O ground state potential energy scan presented in Figure S3, there are two ΔE_{90}. From left to right, the first transition state barrier is the first barrier to perpendicularity (ΔE_{90}=643 cm^{-1}). The second transition state barrier is ΔE_0, which is equal to 887 cm^{-1}. The third transition state barrier is the second $\Delta E_{90,}$ which is equal to 1,818 cm^{-1}. At 140˚, there is a local minimum in a semi twisted configuration. The first ΔE_{90} is smaller than ΔE_0 by about 250 cm^{-1}, while the second ΔE_{90} is larger by ΔE_0 by about 930 cm^{-1}. From examining the transition state geometries, the position of the water molecule changes across the dihedral angle scan. At the ΔE_{90}

with a lower value, the two water molecules are positioned more directly over the pyrrole ring, whereas at the higher-energy ΔE_{90}, the water molecules interact with the phenyl ring. The difference between the local and global minima is also due to solvent position, where at 140˚ the water is located above the phenyl ring and at 220˚ the water is interacting with the pyrrole ring. The importance of water solvent in facilitating charge transfer and changing the barriers to twisting will be more fully explored in the Discussion section.

From the 1PhPy + $2H_2O$ potential energy scan in the excited state (Figure S3), ΔE_0 is equal to 1,549 cm^{-1} and ΔE_{90} is equal to 791 cm^{-1}. The energy minimum has a dihedral angle of 114˚, which is closer to a perpendicular rather than planar conformation. When adjusted to a value between 0-90˚, this becomes the 74.1 values reported in Table 2. The barriers to twisting are not located at 0˚ or 90˚, indicating that while the molecule may exist in a planar or perpendicular geometry in a local minimum, it may not easily be able to convert between the two. Again, the lowest-energy geometry is consistent with the bent geometry found for the 1PhPy bare chromophore and 1PhPy + H_2O.

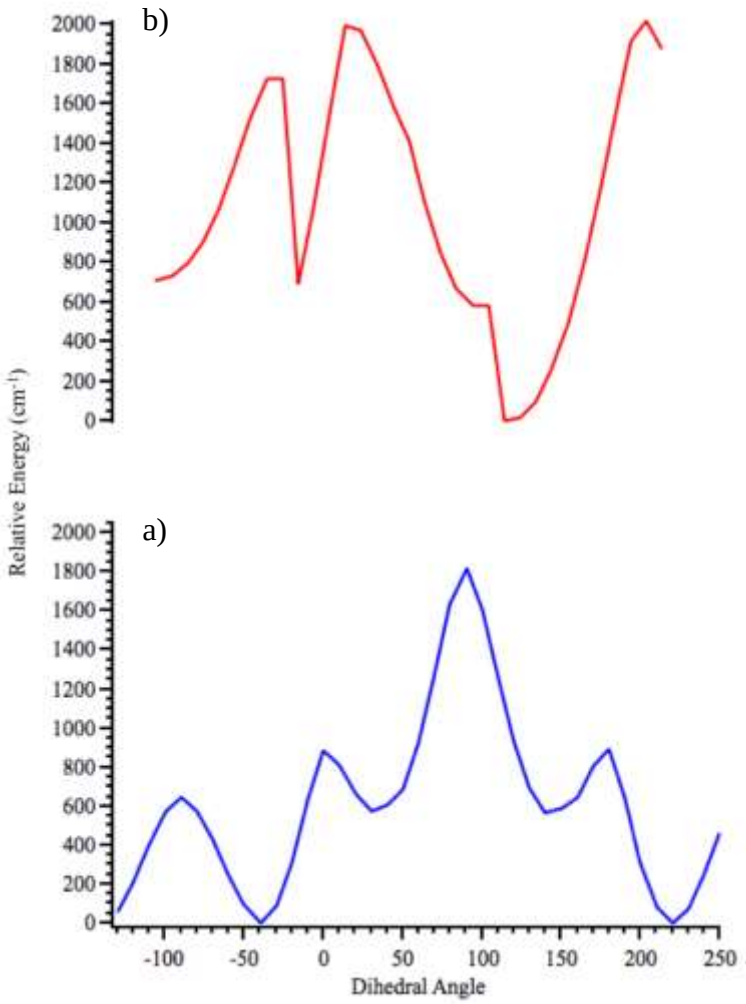

Figure S3: Potential energy surfaces of 1PhPy + 2H_2O in the (a) ground and (b) excited state.

Similar to the 1PhPy + 2H_2O molecular complex, there are multiple barriers to perpendicularity and planarity found for the 1PhPy + 3H_2O ground state potential energy surface shown in Figure S3a. The two ΔE_{90} are equal to 1,397 cm^{-1} and 900 cm^{-1}, corresponding to the first and fourth transition state barriers in Figure S3a. The ΔE_0 are equal to 1,887 cm^{-1} and 461 cm^{-1}, corresponding to the second and third barriers in Figure S3a. Upon closer inspection, the barriers to planarity and perpendicularity may be due to the migration of the water molecules as the dihedral angle changes. In particular, the higher-energy barriers are associated with the water molecules

arranging themselves between the two aromatic rings or localized on the phenyl ring. However, the 1PhPy + $3H_2O$ geometries with lower-energy barriers reveal more localized interaction with the pyrrole unit of 1PhPy. We will discuss this point in further detail as it relates to charge transfer in the Discussion section.

The potential energy surface for the excited state of 1PhPy + $3H_2O$ in Figure S4 is unique in that the excited state barriers are lower in energy than the corresponding ground state barriers. Since the optimal structure for the excited state has a dihedral angle at 90˚, motion to overcome perpendicularity is barrierless ($\Delta E_{90} = 0$). Furthermore, ΔE_0 is approximately 1100 cm^{-1} for structures at both 0˚ and 180˚.

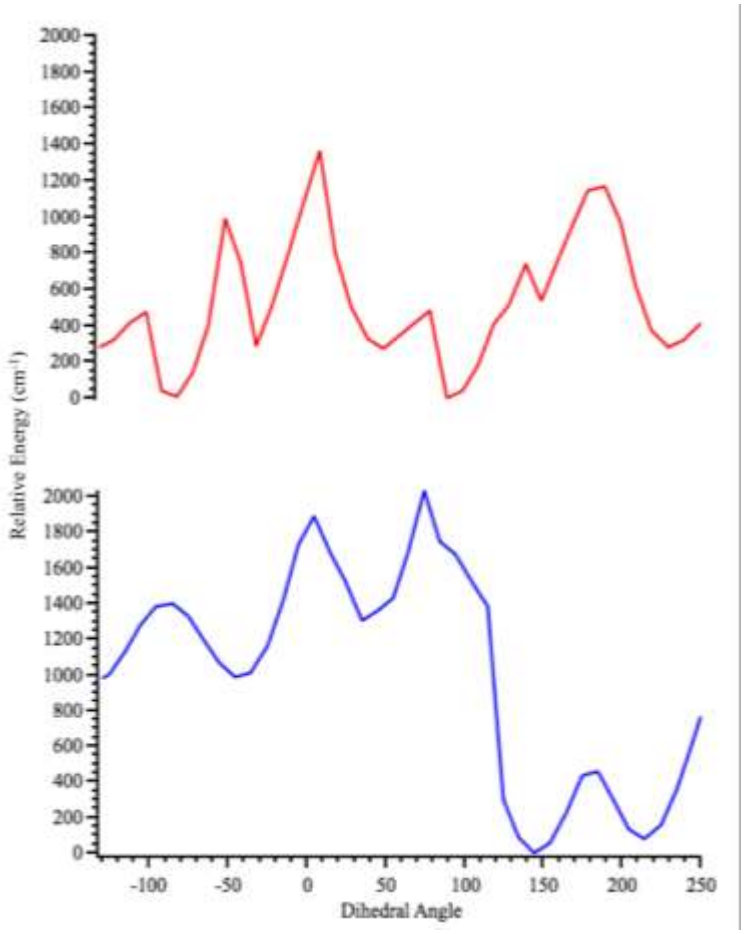

Figure S4: Potential energy surfaces of 1PhPy + $3H_2O$ in the (a) ground and (b) excited state.

1D-DVR Simulations of Spectra on Purely Electronic Torsional Potential Energy Surfaces

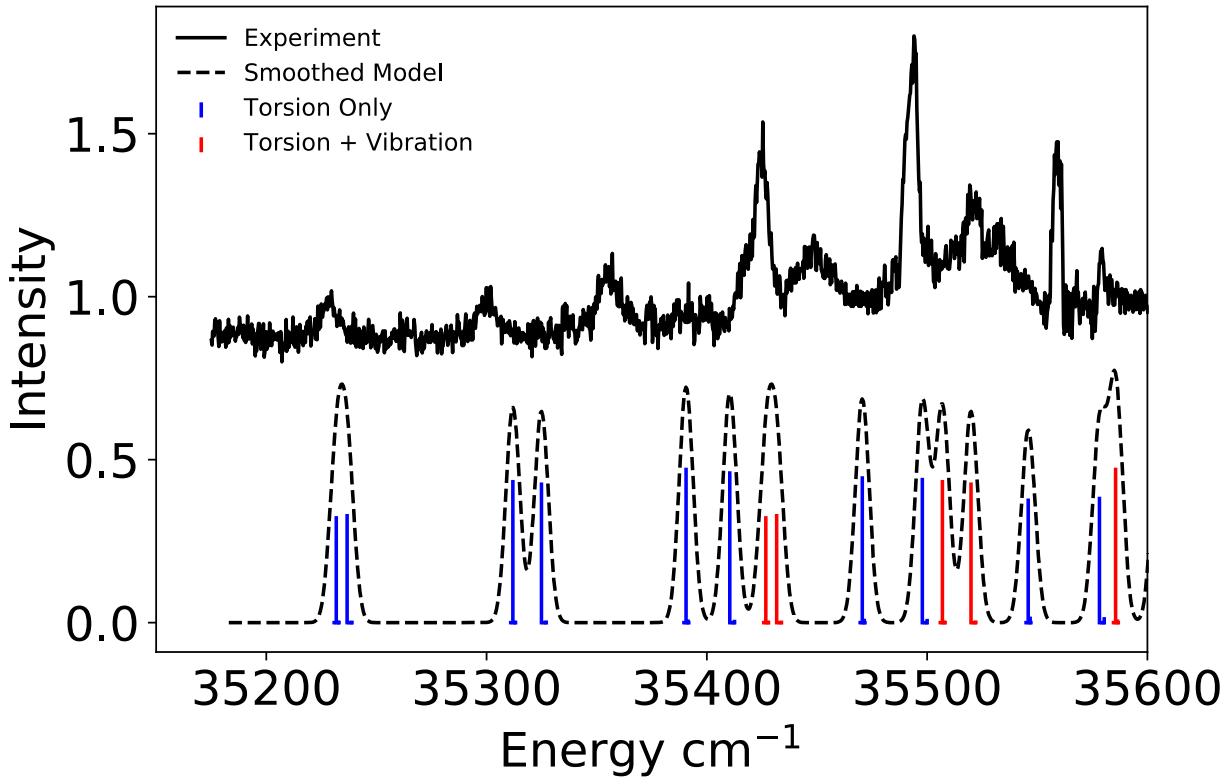

Figure S5) Calculated spectrum for the 1PhPy + 1H_2O complex plotted against the experimental spectrum. The spectral fitting follows the same procedure as in the main text, but the pure electronic energy (Figure S2) torsional potential energy surfaces are used instead of accounting for zero-point effects of the "faster" vibrational modes.

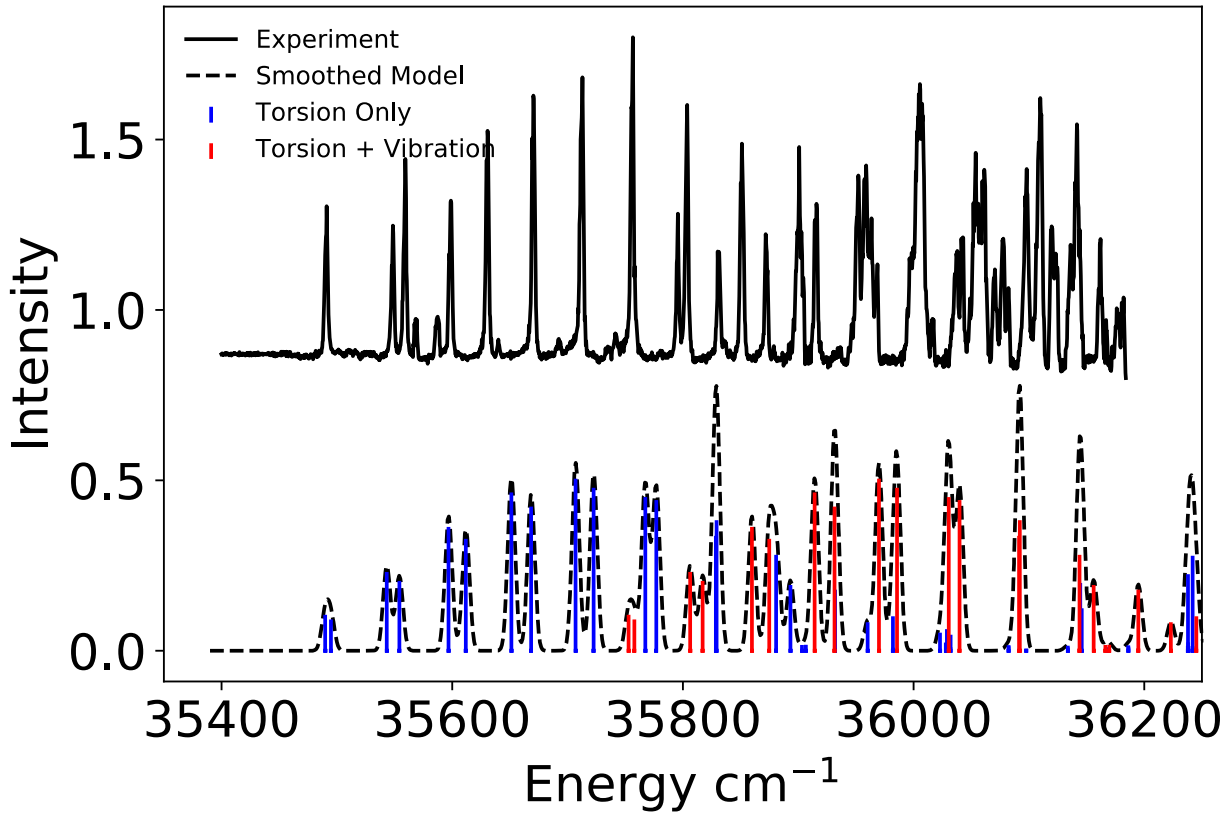

Figure S6) Calculated spectrum for the 1PhPy plotted against the experimental spectrum. The spectral fitting follows the same procedure as in the main text, but the pure electronic energy (Figure S1) torsional potential energy surfaces are used instead of accounting for zero-point effects of the "faster" vibrational modes. As with the fit in the main text, the spectrum continues on to higher energies.

Example Plots of Calculated Torsional Wavefunctions

PhPy + 1H_2O *Ground Electronic State*

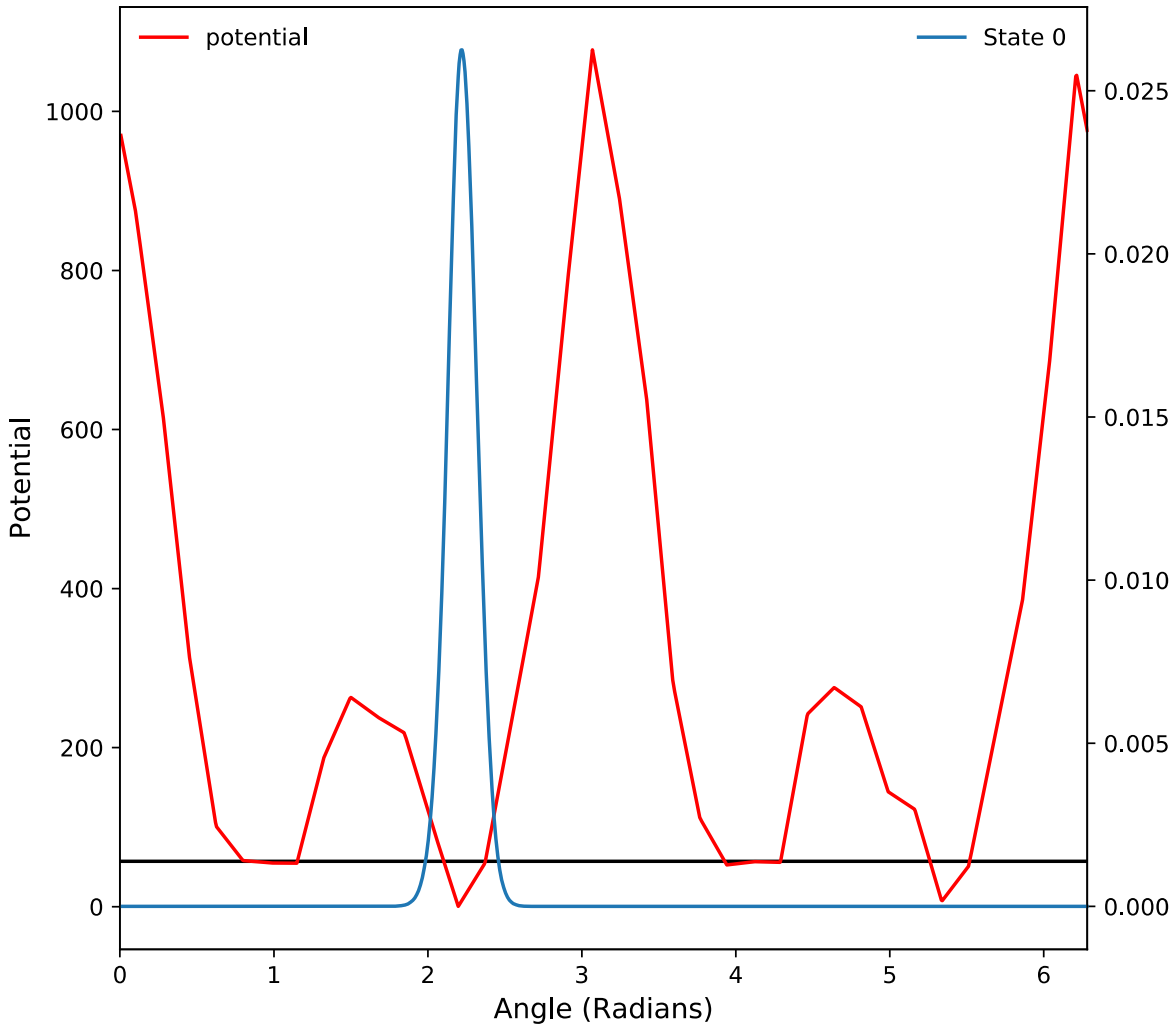

Figure S7: Ground state torsional wavefunction for the 1PhPy + 1H_2O complex. The wavefunction is localized due to the discretization and open interval of the DVR procedure.

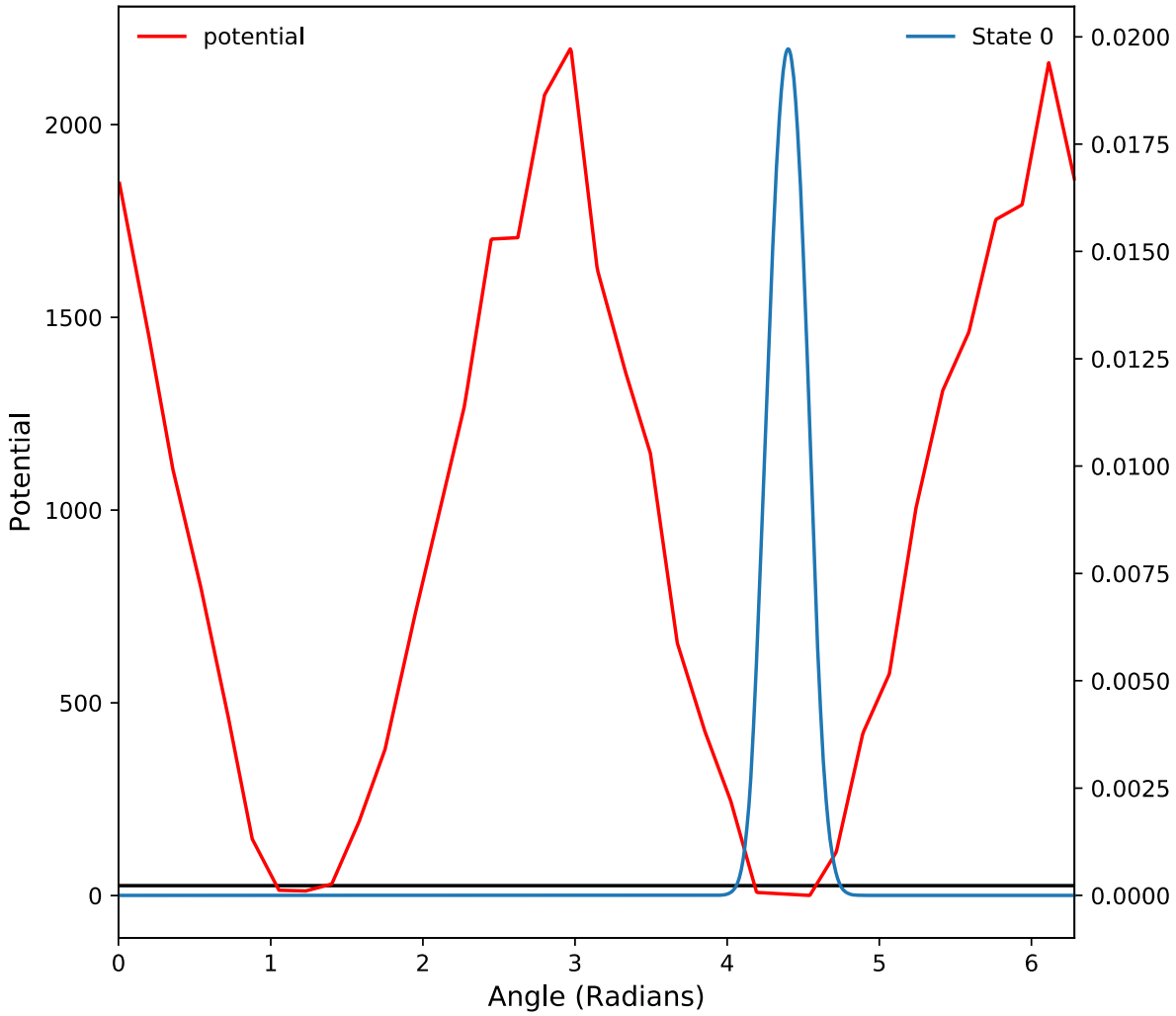

Figure S8: Electronically excited state torsional wavefunction for the 1PhPy + 1H_2O complex.

The raw values for the potential energy surface and the wavefunctions for all potentials are provided as .dat files in the Github repo (https://github.com/Tabor-Research-Group/phenylpyrole-dvr). The first column is the value in radians and the second column is the value of the wavefunction and or fitted potential at that point.